JOURNAL OF GEOPHYSICAL RESEARCH, VOL. 90, NO. A11, PAGES 10,875–10,895, NOVEMBER 1, 1985

An ISEE 3 Study of Average and Substorm Conditions in the Distant Magnetotail

J. A. SLAVIN,[1] E. J. SMITH,[1] D. G. SIBECK,[2] D. N. BAKER,[3]
R. D. ZWICKL,[3] AND S.-I. AKASOFU[4]

Average and substorm conditions in the lobe and plasma sheet regions of the earth's magnetotail are studied as a function of downstream distance and east-west location using ISEE 3 magnetometer and plasma analyzer measurements. On the basis of 756 magnetopause crossings a low-latitude magnetotail diameter of 60 ± 5 R_E at $|X| = 130$–225 R_E is determined. The strength of the lobe magnetic field from $|X| = 20$ to 130 R_E is shown to fall off as $X^{-0.53 \pm 0.05}$. Flaring ceases on average at $|X| = 120 \pm 10$ R_E with a relatively constant $B_L = 9.2$ nT beyond that distance. The ratios $|B_y/B_x|$ and $|B_z/B_x|$ in the translunar tail lobes are small and relatively constant with mean values of 0.10 and 0.06, respectively. These results are shown to be in good agreement with the Coroniti-Kennel flaring tail models of lobe magnetic field configuration with slightly enhanced B_y due to Maxwell stresses exerted at the magnetopause by the solar wind. The plasma parameters V_x, n_e, β_e, and M_A in the lobes all increase with distance down the tail while T_e decreases. The mean values of these lobe quantities at $|X| = 200$–220 R_E are $V_x = -200$–250 km/s, $n = 0.1$–0.2 cm^{-3}, $\beta_e = 0.02$–0.05, $M_A = 0.3$–0.4, and $T_e = 5$–8×10^5 °K. Strong density and weak velocity and temperature gradients are observed as ISEE 3 moves from the center of the lobes out toward the magnetopause. In particular, factor of 3–6 increases in plasma density are observed as the spacecraft moves from the center of the tail at $|Y'| < 10$ R_E (Y' refers to the aberrated GSM system) toward the dawn and dusk portions of lobes at $|Y'| > 20$ R_E. Good agreement is found between the leaky magnetopause model of Pilipp and Morfill (1978) and the strong density/weak velocity gradients observed in the lobes. Substorm activity, as measured by $AE(9)$, is only weakly correlated with magnetic field strength, electron beta, or Alfvénic Mach number in the lobes at $|X| > 200$ R_E. The plasma sheet magnetic field intensity and electron temperature decrease with increasing downstream distance, while flow speed, density, and Alfvénic Mach number all increase. Average plasma sheet parameters at $|X| = 200$–220 R_E are $B = 4.0$ nT, $V_x = -500$ km/s, $n_e = 0.3$ cm^{-3}, $T_e = 1.2 \times 10^6$ °K, and $M_A = 2.7$. Electron beta is independent of downstream distance with a mean value of approximately 0.7. On the basis of pressure balance arguments the estimated total plasma beta in the $|X| > 60$ R_E plasma sheet is 4.5, and the T_i/T_e ratio is 5.5. With respect to reconnection, the most significant results are the correlations between B_z, V_x, and $AE(9)$ in the plasma sheet, the variation in these parameters with X and $\pm Y$, and their implications for the location of the distant neutral line. The highest tailward flow speeds are found to be proportional to the magnitude of the embedded southward B_z. Furthermore, both tailward V_x and southward B_z are shown to be well correlated with $AE(9)$. Earthward of $|X| = 100$ R_E the average B_z is northward and the flow is on average sub-Alfvénic. Between $|X| = 100$ and 180 R_E the flow becomes predominantly tailward and super-Alfvénic, $M_A = 1$–2, across the entire width of the tail. However, the average magnetic field is found to be southward only in a 10 R_E wide region near the aberrated noon-midnight meridian. At $|X| = 180$–225 R_E the flow speed is somewhat higher, $M_A = 2$–3, and the width of the region of southward B_z grows to 30 R_E. Tailward flow speed and electron temperature exhibit maxima in the central portion of the plasma sheet where $B_z < 0$. However, at $|Y'| > 15$ R_E, where $B_z > 0$, the flow direction remains tailward, albeit at a reduced speed. The magnetic field results are interpreted in terms of a curved distant neutral line which is located at $|X| = 100$–140 R_E near local midnight. Along the flanks of the magnetotail closed field lines are apparently still being swept tailward at $|X| = 200$ R_E. In summary, there is general agreement between the ISEE 3 magnetic field and plasma measurements in the distant magnetotail and many of the predictions of reconnection theory, but the existing theoretical models will have to be extended to three dimensions before these observations can be fully understood.

INTRODUCTION

Since its discovery [*Smith*, 1962; *Ness*, 1965] the existence and structure of the magnetotail have exerted considerable influence on our understanding of the magnetosphere. Reconnection-based models of the magnetosphere [*Dungey*, 1961, 1965] required that the earth have a long, 1000 R_E, magnetic tail composed mostly of "open" field lines connected to the interplanetary magnetic field (IMF). The purely "viscous" models of the solar wind–geomagnetic field interaction [*Axford and Hines*, 1961] predicted a "closed" magnetosphere with a tear drop shape which terminates at downstream distances of a few tens of earth radii. Evidence, largely indirect, accumulated over the last 2 decades has demonstrated that reconnection dominates the solar wind–magnetosphere interaction (see the review by *Cowley* [1982]). The open models have also been supported by the Pioneer 7, Pioneer 8, and ISEE 3 observations of a well-ordered, bilobed tail at $|X| = 1000$, 500, and 200 R_E, respectively [*Bavassano et al.*, 1974; *Walker et al.*, 1975; *Bame et al.*, 1983; *Slavin et al.*, 1983].

The important role of the magnetotail in substorm processes has also been recognized for a long time [*Atkinson*, 1966; *McPherron*, 1970; *Russell and McPherron*, 1973]. While many aspects of tail dynamics remain poorly understood [*Frank and Ackerson*, 1979; *Hones*, 1979; *McPherron*, 1979; *Heikkila*, 1984], it is well accepted that substorms are powered by the rapid dissipation of magnetotail energy derived from

[1] Jet Propulsion Laboratory, California Institute of Technology, Pasadena.
[2] Department of Atmospheric Sciences, University of California, Los Angeles.
[3] Los Alamos National Laboratory, New Mexico.
[4] Geophysical Institute, University of Alaska, Fairbanks.

Paper number 5A8522.
0148-0227/85/005A-8522$05.00

the solar wind [e.g., *Caan et al.*, 1973; *Perreault and Akasofu*, 1978]. Inside the orbit of the moon, extensive investigations of magnetotail structure and dynamics have been carried out [e.g., *McPherron et al.*, 1973; *Nishida and Nagayama*, 1973; *Hones et al.*, 1976; *Frank et al.*, 1976; *Lui et al.*, 1977; *Caan et al.*, 1979; *Nishida et al.*, 1981; *Hayakawa et al.*, 1982; *Bieber et al.*, 1984]. In particular, the correlations between earthward and tailward plasma sheet flow and the north/south polarity of the embedded field predicted by reconnection theory were sought, but the results have often been inconclusive [e.g., *Lui et al.*, 1977; *Nishida and Russell*, 1978]. However, the near tail is a difficult region for such studies because of the dynamics associated with substorms. Thinning and thickening of the plasma sheet in conjunction with the onset and tailward retreat of neutral lines presents a formidable obstacle to the interpretation of measurements from a single spacecraft. As we shall see later, the ISEE 3 distant geotail mission has the important advantage of spending relatively long intervals of time tailward of the region where reconnection occurs.

The purpose of this study is to further our knowledge of the nightside magnetosphere through analysis ISEE 3 distant tail measurements. In particular, our investigation adds to other recent ISEE 3 studies [e.g., *Bame et al.*, 1983; *Slavin et al.*, 1983; 1984*a*, *b*; *Cowley et al.*, 1984; *Cowley*, 1984; *Siscoe et al.*, 1984; *Hones et al.*, 1984*a*, *b*; *Gloeckler et al.*, 1984; *Klecker et al.*, 1984; *Scholer et al.*, 1984*a*, *b*, *c*; *Sibeck et al.*, 1985*a*, *b*; *Scarf et al.*, 1984; *Smith et al.*, 1984; *Tsurutani et al.*, 1984*a*, *b*, *c*; *Baker et al.*, 1984*a*, *b*; *Sanderson et al.*, 1984; *Daly et al.*, 1984*a*, *b*; *Zwickl et al.*, 1984] in two important ways. First, both plasma and magnetic field observations are analyzed in parallel to a greater extent than previous studies. This approach enables us to compare and contrast the evolution of particles and fields with distance down the tail as well as examine joint plasma parameters such as Mach number and beta. Second, this investigation uses a nine-station *AE* index to assess the dependence of conditions in the distant magnetotail upon substorm activity. Previous ISEE 3 studies have been limited to performing either case studies on the effects of individual substorms or using planetary indices such as *Kp* which possess low temporal resolution and are only moderately sensitive to substorm current systems.

Accordingly, the main objectives of the study are (1) to examine the average magnetic field and plasma conditions in the tail as a function of radial distance from the earth and east-west distance from the X axis and (2) to extend the previous studies of substorm dynamics into the translunar magnetotail. As will be shown, the results of this investigation lend strong support to the flaring tail models of magnetopause geometry, to the open models of the magnetosphere, and to the reconnection models of the substorm process.

ISEE 3 MEASUREMENTS

For the purpose of this study we have assembled a 5-min averaged merged data set of ISEE 3 magnetic field [*Frandsen et al.*, 1978] and plasma measurements [*Bame et al.*, 1978]. The Jet Propulsion Laboratory vector helium magnetometer makes six magnetic field measurements per second, while the Los Alamos National Laboratory (LANL) plasma analyzer performs a 3-s electron measurement every 84s. Figure 1 presents an example of the ISEE 3 measurements over an interval when tail motion caused the spacecraft to pass through the main regions of the tail. Unless stated otherwise, this study treats the magnetic field measurements in GSM coordinates. A detailed discussion of the methods used to derive bulk plasma parameters from the electron measurements and their limitations is contained in the work of *Zwickl et al.* [1984]. For the purposes of this study, the principal caveat is that intervals with flow speeds of less than 100–150 km/s may have poorly determined bulk plasma parameters.

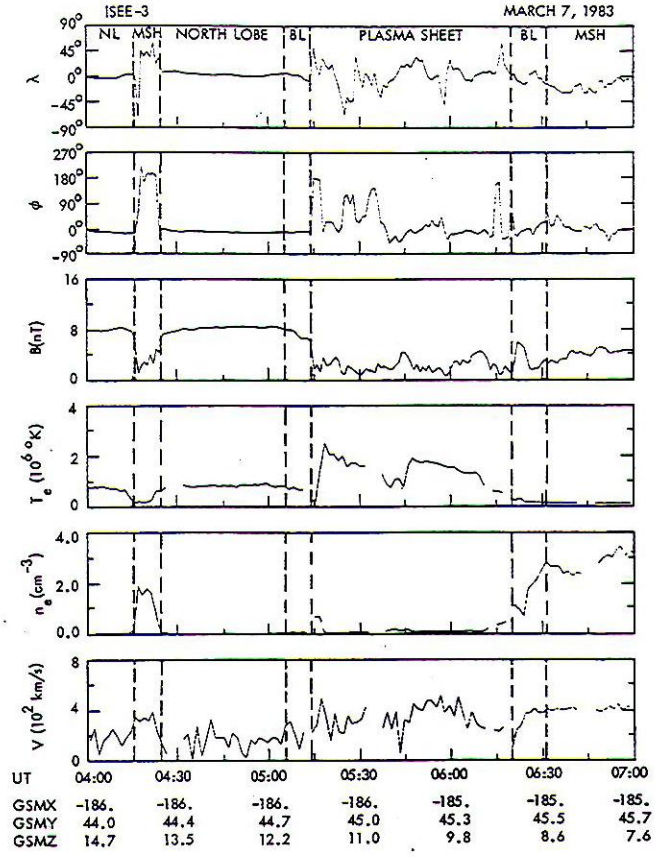

Fig. 1. An example of the ISEE 3 magnetic field and plasma observations in the distant magnetotail. The magnetic field observations are 1-min averages, and they are displayed in the GSM coordinate system. The magnetosheath is marked as MSH, and boundary layers are marked by BL.

The first region encountered in Figure 1 is the north lobe. As was discussed in the earlier ISEE 3 publications [e.g., *Bame et al.*, 1983; *Slavin et al.*, 1983; *Tsurutani et al.*, 1984*b*; *Zwickl et al.*, 1984], the lobes of the distant tail are low beta regions filled with relatively strong, low-variance magnetic fields pointing essentially toward (north lobe) or away (south lobe) from the earth. Following a brief encounter with the magnetosheath, and the north lobe again, first the plasma sheet boundary layer and then the plasma sheet proper are entered. As the spacecraft passes into the boundary layer region, density slowly rises, the magnetic field weakens, and the field variance increases over that observed in the lobes. Shortly thereafter a sudden decrease in field strength occurs in conjunction with increases in plasma density, temperature, and velocity as ISEE 3 enters the plasma sheet. Finally, starting around 0620 UT there is a very gradual exit from the tail through the low-latitude boundary layer separating the plasma sheet and magnetosheath. In this particular case the magnetic field showed little variation across the magnetopause except for a slow increase in strength. The plasma measurements displayed a larger jump with density increasing to several per cubic centimeter, speed becoming steady near 400 km/s, and the electron temperatures falling to 1–1.5 × 10^5 °K.

These examples of the ISEE 3 tail measurements call attention to the complementary nature of the plasma and field observations and the need to use them together in studies of tail structure. The magnetic field data allow the lobes to be readily identified, but the magnetosheath can sometimes, depending upon IMF direction and the variance levels, appear very much like the plasma sheet. Similarly, while the density and temperature differences generally make it easy to separate the plasma sheet and magnetosheath regions, the broad plasma sheet boundary layers can make it difficult to mark precisely the lobe–plasma sheet interface in the plasma data.

DIMENSIONS OF THE TAIL

In Figure 2 the ISEE 3 trajectory for the time interval of this study, December 25, 1982, through April 20, 1983, is displayed in both GSE and GSM coordinates. For reference, the Explorer 33 and 35 magnetopause model of *Howe and Binsack* [1972] is also shown. The model has been rotated in the X-Y plan by 4° to take into account aberration due to the motion of the earth. As is shown, this period is composed of two ISEE 3 orbits with apogees near 80 and 220 R_E. The east-west and north-south limits on ISEE 3's trajectory relative to the aberrated X axis were approximately ± 35 R_E and ± 10 R_E, respectively, in the GSE frame. The second deep tail orbit was not considered by this study because all of the processed data were not yet available. However, the spatial coverage is basically similar but with some increase in the north-south coverage and a slightly greater apogee, 238 R_E.

IMP 8 returned interplanetary measurements for much of the time period covered by this study and observed variations in flow speed of 200–800 km/s and $\pm 5°$–10° in direction (A. Lazarus, private communication, 1983). The full range of flow speed variations will affect tail aberration angle by about $\pm 3°$, which corresponds to ± 10 R_E along the Y axis at $|X| = 200$ R_E. The envelope of solar wind flow directions should produce movement along the Y and Z axes at $|X| = 200$ R_E of ± 17–35 R_E. The net result is that any fixed point within the tail at $|X| = 200$ R_E will be moved around by the solar wind within an ellipse in the Y-Z plane with east-west dimensions of ± 27–45 R_E and north-south extent of ± 17–35 R_E. Because the region over which the solar wind moves the tail exceeds the Y-Z range of the ISEE 3 trajectory, it becomes impossible to determine the location of the spacecraft relative to the tail at any given time simply on the basis of spacecraft location. All tail features (e.g., magnetopause, neutral sheet, lobes, plasma sheet, mantle, plasma sheet boundary layer, etc.) may be observable, least on occasion, along the entire ISEE 3 trajectory.

As part of a separate study, 756 magnetopause crossings have been identified in the magnetic field and plasma observations during the first 90 days of 1983 [*Sibeck et al.*, 1985*b*]. The locations of these crossings have been plotted as tick marks along the ISEE 3 orbits in the GSE panels of Figure 2. Both the number of crossings and the number of days spent in the various intervals are displayed. As would be expected from the preceding discussion, magnetopause crossings were observed over the entire ISEE 3 distant tail trajectory. Because the amplitude of the tail motion associated with solar wind variations exceeds one tail radius, the frequency of magnetopause crossings was high even in the center of the tail near apogee. In this region, solar wind induced motion of the tail can bring the spacecraft into contact with the magnetopause from any direction, although encounters with the southern portion of the magnetopause surface were favored because ISEE 3 was 10 R_E below the ecliptic. Failure to take into account the magnitude of the lateral motion of the tail at these downstream distances can result in the tail appearing filamentary, as was reported by some of the early Pioneer 7 and 8 papers (see reviews by *Villante* [1977] and *Cowley* [1984].

Under these circumstances the determination of the average dimensions of the tail can become difficult. However, close inspection of the crossing distributions relative to the *Howe and Binsack* [1972] model, based upon observations at $|X| < 100$ R_E, does show a clustering of the encounters about the locations where the spacecraft is predicted to have crossed the magnetopause. The frequency of magnetopause encounters falls off from 10–20 per day near the predicted position of the magnetopause to 5–10 per day when ISEE 3 moved significantly inside or outside of the model surface. Accordingly, there appears to be reasonable agreement between the ISEE 3 magnetopause crossings and the extrapolated Howe and Binsack model which predicts a tail diameter of about 60 R_E.

The locations of the ISEE 3 magnetopause crossings at $|X| = 130$–225 R_E are also dislayed as histograms in Figure 3. In Figure 3*a* the crossings have been aberrated by 4.5° and placed into 5 R_E bins along the rotated Y axis (i.e., Y'). The regions not sampled by the ISEE 3 orbit are indicated by the slant line shading. While magnetopause crossings are observed at all locations, the most probable magnetopause positions are just inside $Y' = \pm 30$ R_E. This result is emphasized in Figure 3*b* where the crossings are binned against $|Y'|$; again, the most probable tail radius is about 30 R_E. Finally, in Figure 3*c* the actual distance from the X' axis to each of the crossings, $(Y'^2 + Z'^2)^{1/2}$, is displayed with a resultant radius of just over 30 R_E. On the basis of both the comparison with the Howe and Binsack model in Figure 2 and the histograms in Figure 3, we conclude that the average low-latitude (i.e., east-west) diameter of the magnetotail is 60 ± 5 R_E.

AVERAGE LOBE CONDITIONS

For the December 25, 1982, to April 20, 1983, period considered by this study, all distinct lobe and plasma sheet regions were identified by hand using the same criteria as discussed in connection with Figure 1 [see *Bame et al.*, 1983; *Slavin et al.*, 1983]. Simply stated, intervals containing strong, low-variance magnetic fields, oriented toward/away from the earth, with low plasma densities were identified as tail lobe regions. Plasma sheet intervals corresponded to regions adjacent to the lobes which contained weak, high-variance magnetic fields, and hot plasmas with densities intermediate between the lobe and magnetosheath values. *Zwickl et al.* [1984] codified a set of region definitions in the form of a computer algorithm for the identification of tail regions. Such an approach has a number of advantages including speed of application and objectivity for a given set of definitions. However, in nearly all cases examined the intervals identified as lobe or plasma sheet by this study were similarly labeled by the Zwickl et al. algorithm. The main difference between the two approaches is that the Zwickl algorithm makes no attempt to differentiate between the boundary layers and the plasma sheet/lobe regions proper. For this study we have excluded the boundary layers whenever sufficient plasma was present to cause about a 10% decrease in magnetic field strength. In addition, to further discriminate against the boundary layer regions only lobe and plasma sheet intervals greater than about 15 min were included to limit the number of times these layers were transversed per unit time in the lobe or plasma

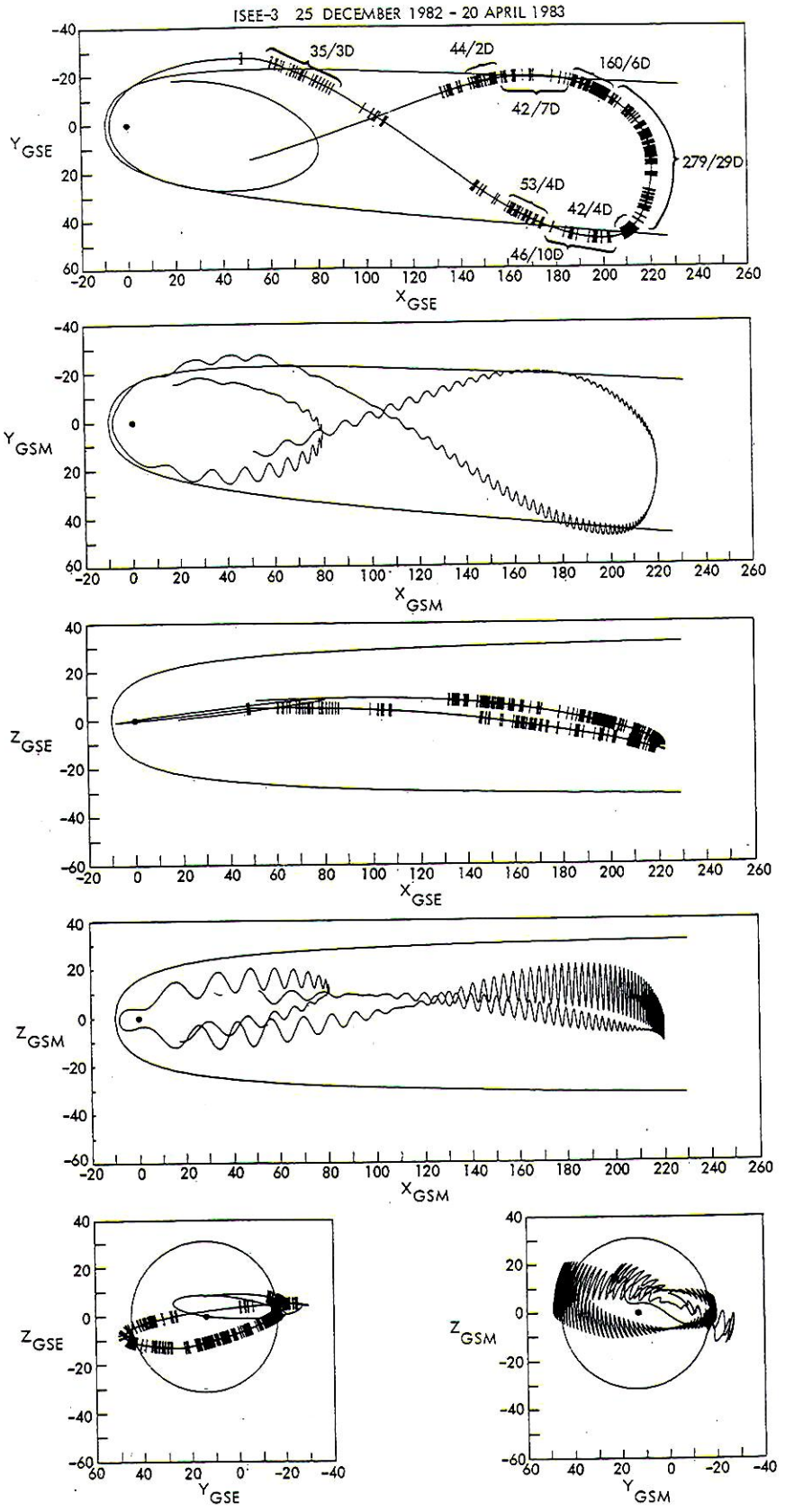

Fig. 2. The ISEE 3 trajectory during the interval considered by this study (December 25, 1982, to April 20, 1983) is plotted in both GSE and GSM coordinates. Hours in which magnetopause crossings took place are marked with ticks. In regions of interest the total number of crossings identified in the 5-min data set and the length of the interval in days are indicated.

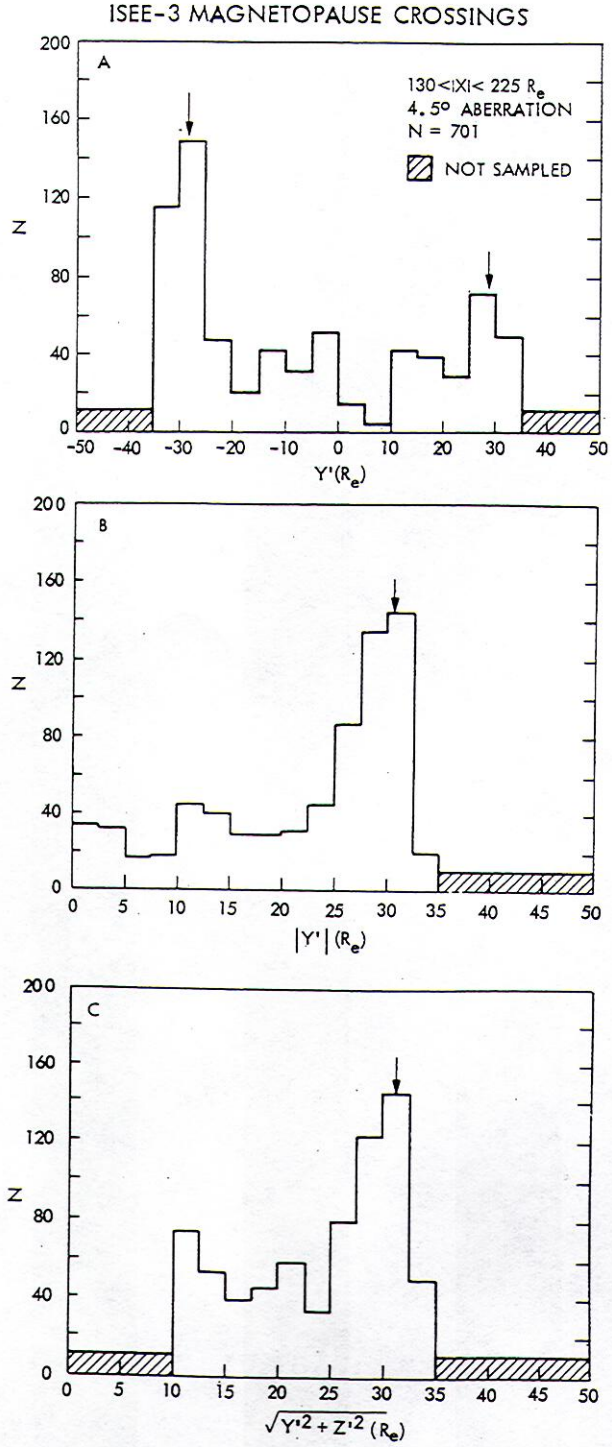

Fig. 3. Histograms of the locations at which the magnetopause was encountered by ISEE 3 between $|X| = 130$ and 225 R_E are displayed in terms of the Y', $|Y'|$, and $(Y'^2 + Z'^2)^{1/2}$ coordinates. The regions not sampled by the ISEE 3 trajectory are marked by the slant line shading. Arrows mark the most probable magnetopause positions.

sheet. While the boundary layers are quite important to our understanding of the tail, we have chosen to consider them separately in other studies [e.g., *Sibeck et al.*, 1985*a*, *b*].

In Figure 4 the 5-min averaged ISEE 3 merged magnetic field and plasma data set is used to examine plasma conditions in the lobes of the magnetotail. The selected parameters are electron beta, $\beta_e = 8\pi n_e k T_e/B^2$, Alfvénic Mach number, $M_A = V/[B/(4\pi n m_p)^{1/2}]$, a measure of the north-south tilting of the magnetic field in GSM coordinates, $|B_z/B_x|$, a measure of the east-west tilting of the magnetic field in GSM coordinates, $|B_y/B_x|$, the total magnetic field intensity B, the electron temperature T_e, the electron density n_e, and the X component of the flow velocity, V_x. These quantities have been averaged by 10 R_E bins between $|X| = 50$ and 230 R_E. The standard errors in the mean are generally comparable in size to the plotting symbols and hence are not displayed. However, in the case of the plasma measurements the parameters determined during intervals of low-speed flow are more uncertain than those for high-speed flow conditions as discussed by *Zwickl et al.* [1984]. The thresholds for reliability determined by Zwickl et al. are indicated with slant line shading at the bottom of the V_x panel. As is shown, the accuracy of the lobe parameters increases with growing downstream distance. The

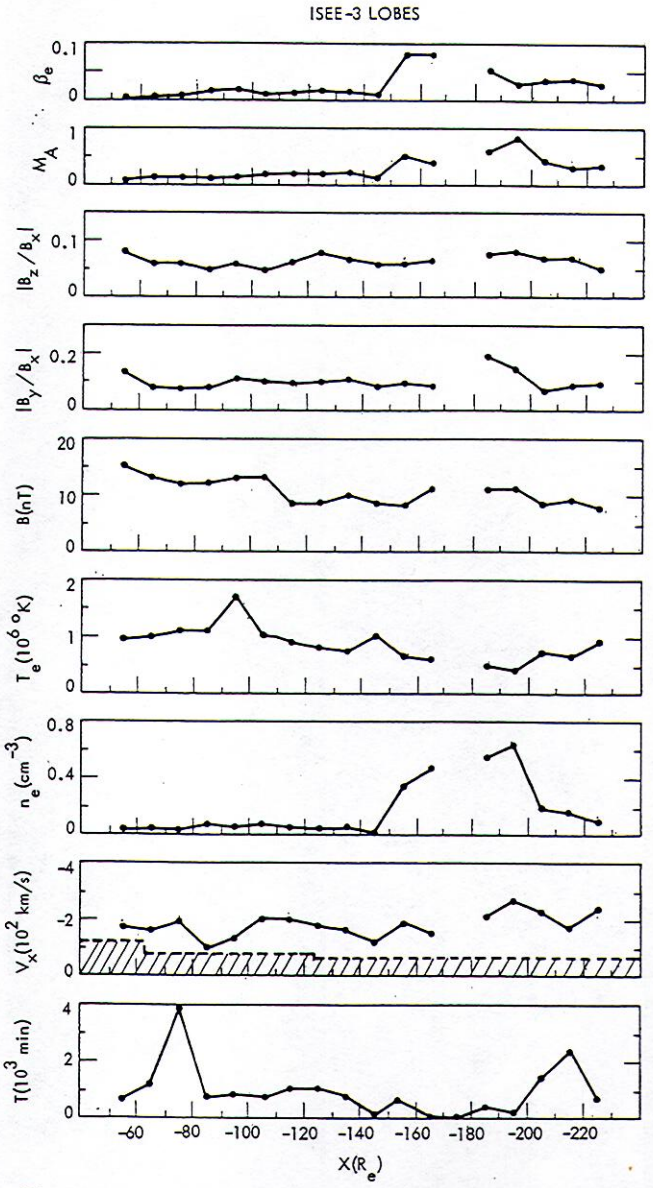

Fig. 4. A set of lobe plasma parameters are plotted as a function of X. Negative V_x corresponds to flow away from the earth. Note the large increase in lobe density when the spacecraft was at $150 < |X| < 200$ R_E. During that interval, ISEE 3 was at its greatest east-west extent in Y, as will be examined in another figure. The bottom panel displays the amount of time the spacecraft spent in each 10 R_E bin.

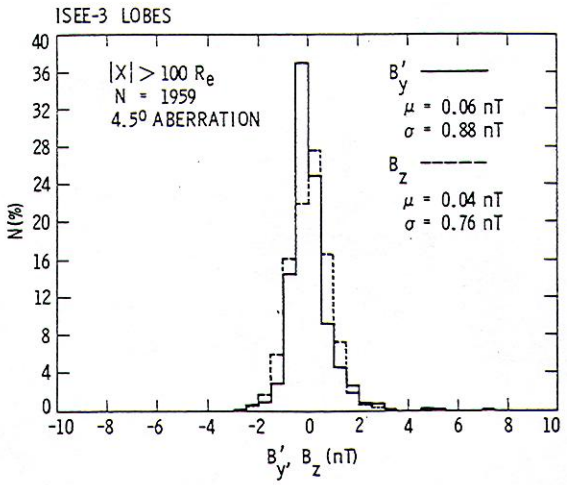

Fig. 5. Histograms of the Y and Z components of the lobe magnetic field in solar-wind-aberrated coordinates are displayed for $|X| > 100\ R_E$. The aberration angle used, 4.5°, was chosen because it produced a B_y' distribution which was approximately centered on zero.

total number of minutes T spent by ISEE 3 in each bin is displayed in the bottom panel. The sampling is lowest closer to the earth, where ISEE 3 was moving faster, and at $|X| = 140\ R_E$ to 200 R_E due to the orbit of the spacecraft taking it into the dawn and dusk magnetosheath. The total number of observations is greatest near $|X| = 80$ and 220 R_E where the spacecraft passed through apogee.

As is indicated, the lobe magnetic field intensity falls from about 15 nT at $|X| = 50\ R_E$ to 8–10 nT at 200–220 R_E in agreement with the earlier study by *Slavin et al.* [1983]. The magnetic field is predominantly along X, as can be seen, for example, in the lobe field distributions published by *Slavin et al.* [1984*b*]. The quantities $|B_z/B_x|$ and $|B_y/B_x|$ are relatively constant beyond the orbit of the moon with values of 0.06 and 0.10, respectively. It is quite reasonable for the ratio $|B_y/B_x|$ to be greater than $|B_z/B_x|$ because the Y component of the field may be enhanced by the effects of aberration as well as changing solar wind flow direction.

In Figure 5 the properties of the lobe magnetic fields are further investigated by first aberrating B_y, to create B_y', and then plotting histograms of B_y' and B_z for $|X| > 100\ R_E$. The mirror symmetry between the north and south lobes allows us to plot the B_z values independent of in which lobe a given measurement was made. However, in the case of B_y' the sign had to be reversed for the observations made in the south lobe. As is displayed, the B_z distribution had a mean value of 0.04 nT, so the mean solar wind flow direction for the ISEE 3 tail observations discussed here was very near the ecliptic. After aberration by 4.5°, the mean B_y' field is also very close to zero, i.e., 0.06 nT. Accordingly, both the magnetopause analysis in Figure 3 and the lobe field measurements indicate that the average solar wind flow speed for this period was approximately (30 km/s)/(tan 4.5°) = 380 km/s. Finally, the standard deviations in the B_y' and B_z distributions were 0.88 and 0.76 nT, respectively. If it is assumed that the primary causes of variance in lobe B_z are changing solar wind flow direction and, perhaps, some small flaring of the field, then these effects can be subtracted from B_y' to obtain an effective residual Y' field of $[(0.88)^2 - (0.76)^2]^{1/2} = 0.44$ nT. Compared with the expected mean IMF B_y at 1 AU of cos (45°) × 6 nT = 4.2 nT, the ratio of lobe B_y to IMF B_y is approximately 10%. Small east-west field components in the lobes have been observed before [*Fairfield*, 1979; *Tsurutani et al.*, 1984*c*] and are believed to be caused by stresses exerted at the magnetopause by open field lines extending into the solar wind [*Cowley*, 1981]. The value of 10% obtained here is actually an upper limit, since changing solar wind flow velocity magnitude may also add variance to the B_y' distribution. However, the result is in good agreement with the ISEE 3 study by Tsurutani et al. which compared directly with IMP 8 IMF measurements. Hence overall the lobes of the distant tail at $|X| > 100\ R_E$ are well represented by solenoidal currents and superposition of weak transverse fields due to the Maxwell stresses exerted on the tail by the solar wind.

Returning to Figure 4, between $|X| = 50$ and 200–220 R_E the lobe plasma density and tailward velocity increase from 0.02 cm^{-3} to 0.1–0.2 cm^{-3} and 150–200 km/s to 200–250 km/s, respectively, while the plasma temperature decreases from about 1×10^6 °K to 5–8 $\times 10^5$ °K. This gradual filling of the lobes with cooler, presumably solar wind plasma is in good agreement with the previous ISEE 3 studies by *Gosling et al.* [1984] and *Zwickl et al.* [1984]. In addition, we have also found that electron beta and Alfvén Mach number increase from 0.002–0.005 to 0.02–0.05 and from 0.1 to 0.3–0.4, respectively, as ISEE 3 moved downstream. Hence there is an overall increase in the relative importance of lobe particle energy density with increasing $|X|$. The ratios of both the electron thermal to magnetic energy density, β_e, and kinetic energy to magnetic energy density, $M_A{}^2$, increase by factors of 2.5 and 6.3, respectively. If these trends with X continue, then the lobe plasma will eventually have significant effects upon the magnetic field intensity, configuration, and stability of the magnetotail. Recent analysis of the Voyager observations [*Lepping et al.*, 1983] have detected a similar filling of the lobes in the distant Jovian tail at $|X| = 9000\ R_J$ [*Grzedzielski and Macek*, 1984].

In addition to the relatively smooth variations in lobe plasma and magnetic field parameters with downstream distance, Figure 4 also displays strong, factor of 6 increases in plasma density at distances of $|X| = 150$ to 200 R_E. The values of density and other parameters beyond that distance appear much as they would have had the variations as a function of X observed earthward of $|X| = 150\ R_E$ continued through to apogee. Based upon these observations, and the trajectory information in Figure 2, we interpret the cause of the large density increase at $|X| = 150$ to 200 R_E as being due to the movement of the spacecraft through a density gradient as it went from the central lobe into the outer lobes.

Figure 6 examines this point directly by plotting the lobe plasma parameters against GSM Y. A vertical dashed line indicates the approximate center of the unaberrated magnetotail. As is shown, lobe plasma density, flow speed, $|B_z/B_x|$, and $|B_y/B_x|$ all increase as ISEE 3 moved from the central lobe into the dawn and dusk regions. For electron temperature the trend reverses with cooler plasma being observed as the magnetopause is approached consistent with the origin of mantle particles being the cooler solar wind plasma. Although our lobe selection criteria exclude the densest portions of the boundary layers adjacent to the plasma sheet and magnetopause, it is clear from Figure 6 that relatively strong spatial gradients exist within the mantle and that the actual densities can be quite high as reported by *Bame et al.* [1983], *Zwickl et al.* [1984], *Gosling et al.* [1984], and *Sibeck et al.* [1985*b*]. Furthermore, in agreement with Sibeck et al., enhancements in the B_y and B_z components of the lobe field correlate with the presence of higher-density mantle plasma.

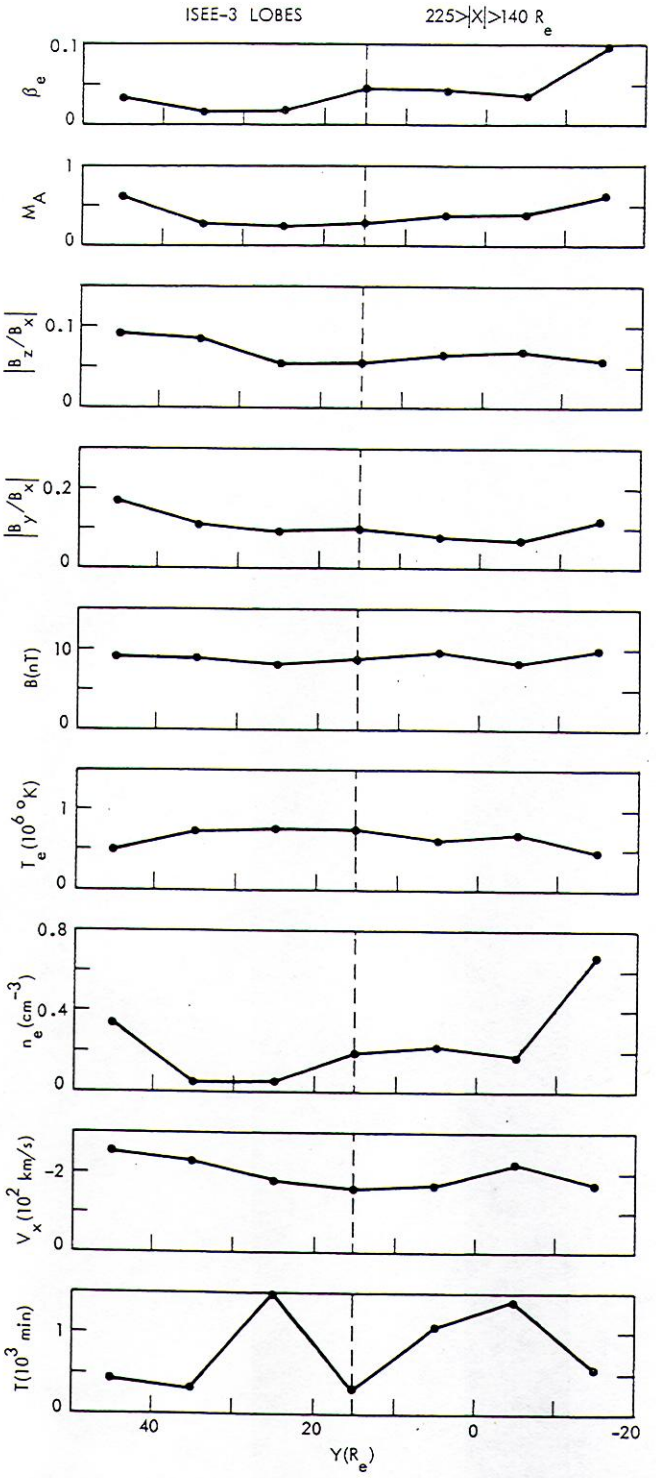

Fig. 6. The same set of lobe plasma parameters as were considered in Figure 4 is plotted as a function of GSM Y over the range $140 < |X| < 225\ R_E$. The vertical dashed line marks the approximate center of the tail under the influence of aberration. Note the factor of 3 to 6 increases in mantle density as the spacecraft moved from the center of the lobes into the dawn and dusk portions of the lobes.

Figure 7 more closely examines the X gradient in magnetic field intensity with a somewhat larger data set of 1-min averaged magnetometer observations. In addition to the intervals contained in the previous figure, this data set also includes the October 20–25, 1982, magnetotail encounter [see *Slavin et al.*, 1983] and the December 23–25, 1982, near-tail portion of the first deep tail orbit not included in the 5-min merged data set. The field falls off rapidly between $|X| = 20$ and $|X| = 110$–$130\ R_E$. On average, therefore, flaring of the magnetopause must cease at a distance of $|X| = 120 \pm 10\ R_E$. Modeled with a power law, the magnetic field strength decreases as $X^{-0.53 \pm 0.05}$. This result is in excellent agreement with the ISEE 3 exponent of -0.54 determined by *Slavin et al.* [1983] with a smaller data set. It is also intermediate between the -0.3 and -0.7 values of *Behannon* [1968] and *Mihalov et al.* [1968] using Explorer 33 observations out to $|X| = 90\ R_E$. A more detailed study of the lobe field gradient is planned for the purpose of better understanding magnetic flux conservation and the evolution of the tail current system with distance. The Explorer 33 magnetic field observations, for example, have been essential in constructing numerical models of the tail [*Birn et al.*, 1977; *Propp and Beard*, 1984]. In particular, corrections must be made for varying external pressure conditions in the solar wind which are directly reflected in the lobe field intensities. At that time it may become appropriate to fit more carefully the gradient in Figure 7 with polynomial expansions or asymptotic functions.

As a tangential discontinuity, magnetopause location corresponds to the equilibrium position between the opposing magnetospheric and solar wind pressures. The pressure balance condition across the lobe–solar wind interface may be written [*Spreiter and Alksne*, 1969; *Coroniti and Kennel*, 1972; *Sibeck et al.*, 1985*a*] as

$$B_L^2/8\pi = nm_pV^2 \sin^2(\psi) + nk(T_i + T_e)_{sw} + B_{sw}^2/8\pi \quad (1)$$

where B_L is the lobe field magnitude, n is solar wind density, V_{sw} is solar wind speed, T_i is solar wind ion temperature, T_e is solar wind electron temperature, ψ is the angle that the normal to the magnetopause makes to the plane normal to the solar wind flow direction, and B_{sw} is the solar wind magnetic field strength. Owing to the low lobe beta values discussed earlier, internal plasma pressure is negligible and has been omitted from the left-hand side of (1). The decrease in lobe field strength with increasing downstream distance occurs in the flaring tail model because of a decrease in flaring angle. A final, or terminal, field strength is reached beyond the point where flaring ceases and the lobe field strength stops decreasing with downstream distance. The terminal lobe field strength may be calculated by setting $\psi = 0°$ and inserting typical solar wind parameter values (i.e., $n = 7\ \text{cm}^{-3}$, $T_i = 8 \times 10^4$ °K,

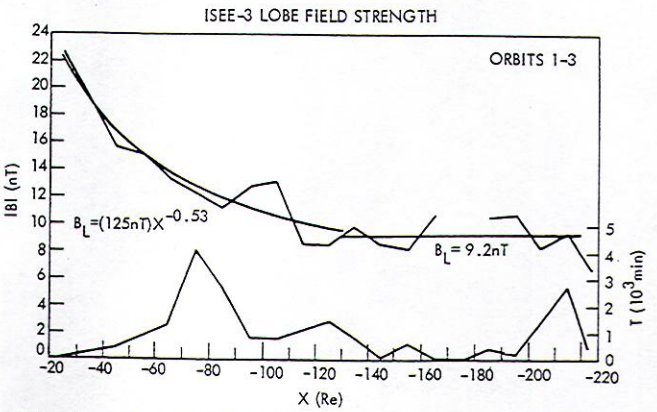

Fig. 7. Lobe magnetic field intensity as a function of X during ISEE 3's first three tail orbits is displayed. The 1-min average data have been modeled with a power law out to $|X| = 130\ R_E$ and a constant value beyond that distance. The total amount of time spent in the lobes as a function of X is shown in the bottom trace.

$T_e = 1.5 \times 10^5$ °K, and $B_{sw} = 6$ nT) into (1). The result is a final lobe field of 9.6 nT, which is in very good agreement with the 9.2-nT terminal field displayed in Figure 7. Furthermore, *Coroniti and Kennel* [1972] have analytically modeled the flaring of the magnetotail. Using their model, *Slavin et al.* [1983] calculated that for average solar wind conditions, flaring should cease very near the $|X| = 110$–130 R_E indicated in Figure 7.

As an additional test of the flaring tail model (i.e., (1)), it is of interest to reconcile the Explorer 35 and lunar surface tail observations at $|X| = 60$ R_E with the ISEE 3 distant tail results. In particular, the 14-nT lobe observed by ISEE 3 at lunar distances (see Figure 7) may be inserted into (1) and combined with average solar wind parameters to solve for the magnetopause flaring angle ψ. The result is a flaring angle of 6.9°. The average diameter of the magnetotail at $|X| = 60$ R_E was well determined by the Explorer 35 lunar orbiter and the Apollo surface experiments and found to be approximately 50 R_E [*Mihalov et al.*, 1970; *Hardy et al.*, 1979]. Assuming a flaring angle of 6.9° and a tail diameter of 50 R_E at lunar distances, the final tail diameter of 60 R_E should be reached near $|X| = 140$ R_E. Given the measurement uncertainties, the long-term changes in solar wind conditions between the Apollo/Explorer 35 epoch and 1983, and the assumption of a single mean flaring angle, the agreement between this result and the $|X| = 110$–130 R_E distance in Figure 7 in quite good. Overall, the results of our study provide very good support for the flaring tail picture of the magnetosphere.

AVERAGE PLASMA SHEET CONDITIONS

The average conditions in the plasma sheet have been examined in the same manner as was applied to the lobe regions in the preceding section. Plasma sheet encounters lasting longer than approximately 15 min were identified on the basis of strong diamagnetic decreases in the strength of the magnetic field and the appearance of hot, dense plasma relative to conditions in the lobes. Plasma sheet parameters averaged by 10 R_E bins are displayed in Figure 8 in the same fashion as for the lobes in Figure 4. However, in making use of the results it must be remembered that the plasma sheet is far more inhomogeneous and time variable than is the case for the lobes. Magnetic field strength, for example, can vary greatly from the outer plasma sheet in to the neutral sheet current layer. In addition, the presence of reconnection, wave turbulence, and plasmoids in the observations will not generally be uniform in X and Y. Accordingly, average plasma sheet parameters must be viewed with far more caution than average models of conditions in the lobes.

As is shown, magnetic field strength in the plasma sheet weakens somewhat with distance beyond the orbit of the moon. At $|X| = 60$ to 100 R_E the mean is 4.9 nT, for 100 to 210 R_E it is 4.4 nT, and finally for $|X| > 210$ R_E the mean field magnitude is 3.7 nT. By comparison, particle density increases gradually by about 50% from about 0.2 to 0.3 cm^{-3}, between $|X| = 30$ and 220 R_E, perhaps in response to the increased supply of cooler mantle plasma with increasing $|X|$ seen in Figure 4. The electron temperature declines by a factor of 2, from 2.5×10^6 to 1.2×10^6 °K. As with the lobe region, these results are in good agreement with *Zwickl et al.* [1984]. Finally, as was discussed earlier, the plasma parameters determined from the electron measurements may be subject to reliability problems in low-speed flows. Slant line shading in the flow speed panel of Figure 8 indicates the thresholds determined by *Zwickl et al.* [1984]. The problem is most severe earthward of

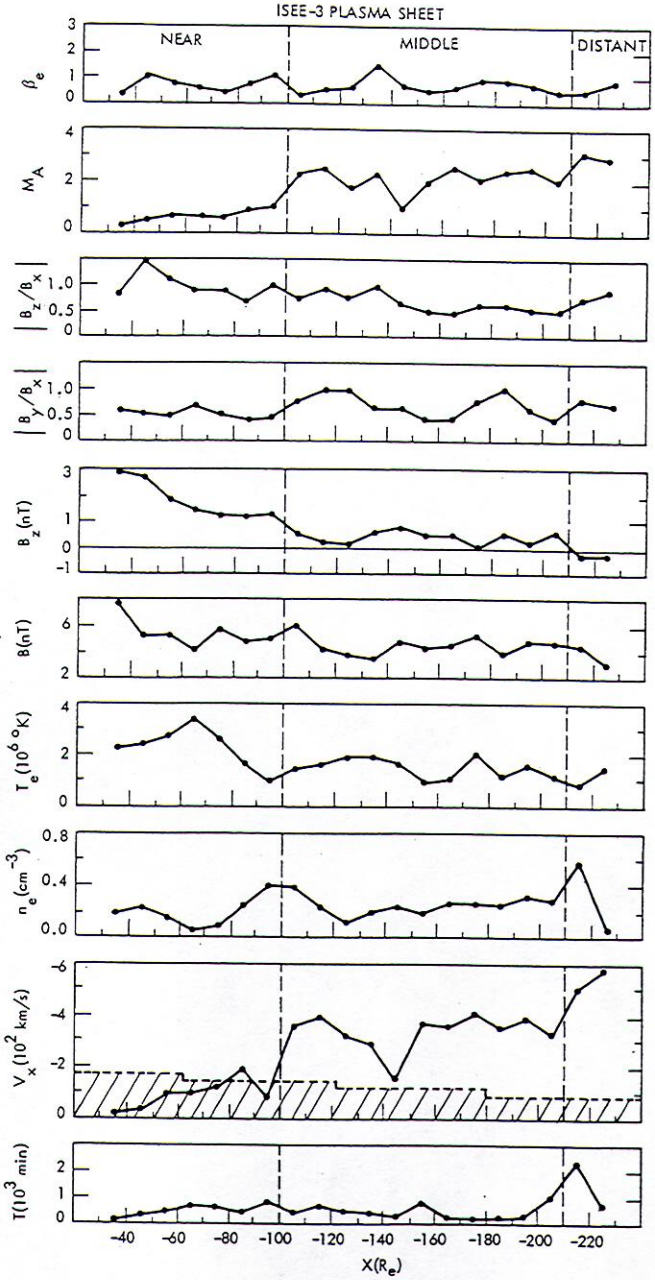

Fig. 8. A set of plasma sheet parameters are plotted as a function of X. In particular, note the onset of super-Alfvénic flow and the sudden decrease in B_z near $|X| = 100$ R_E. The bottom panel displays the total amount of time T the spacecraft spent at each distance.

$|X| = 100$ R_E and when $B_z > 0$, as will be discussed in reference to Figure 13.

The ratio of plasma electron pressure to magnetic pressure, β_e, appears to be independent of $|X|$ with no net change out to apogee. The individual values vary between 0.3 and 1.5. As was mentioned earlier, the ion component of the tail plasma population was not measured by the LANL ISEE 3 instrument. However, by invoking pressure balance between the lobe and plasma sheet regions, total plasma sheet beta, β_{ps}, may be calculated [e.g., *Slavin et al.*, 1984*b*]

$$\beta_{ps} = (B_L/B_{ps})^2 - 1 \quad (2)$$

where B_L and B_{ps} are the magnetic field magnitudes in the lobe and plasma sheet, respectively. In obtaining this ex-

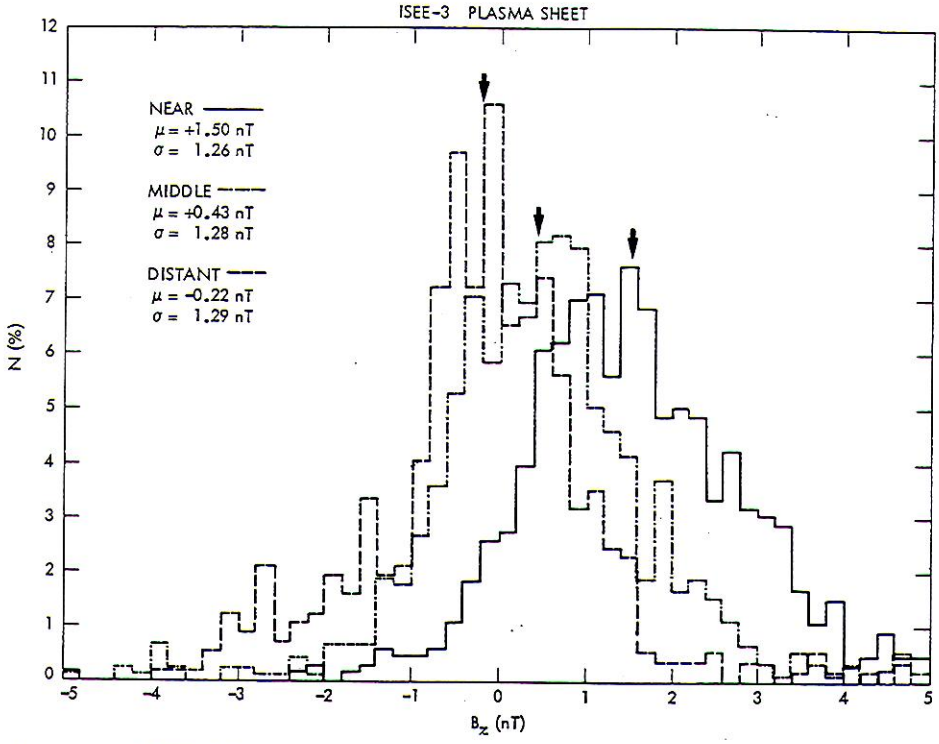

Fig. 9. Histograms of GSM B_z in the plasma sheet are displayed for three distance regimes: near (solid line: $|X| < 100$ R_E), middle (dot-dash line: $|X| = 100$–210 R_E), and distant (dashed line: $|X| > 210$ R_E). The means of the three distributions are indicated with dark arrows.

pression we have assumed that beta in the lobes is much less than unity. Figure 4 indicated that for any plausible ratio of T_i/T_e this should indeed be the case. Also, during intervals when there are large flows into the plasma sheet, such as across reconnection-generated slow shocks [*Feldman et al.*, 1984; *Smith et al.*, 1984], it should be noted that (2) will not always hold true. However, averaged over all times the pressure balance condition and its assumptions should be generally valid. Using the lobe and plasma sheet field magnitudes in Figures 4–8, the inferred plasma sheet beta values are 6.6 at $|X| = 30$–60 R_E, 5.5 at 60–100 R_E, 4.1 at 100–210 R_E, and 4.4 at >210 R_E. Since electron beta is measured directly, the ratio of T_i/T_e in the plasma sheet may be calculated from the inferred total plasma sheet beta:

$$T_i/T_e = (\beta_{ps}/\beta_e) - 1 \quad (3)$$

where it has been assumed that the plasma sheet is predominantly made up of H^+ so that $n_e = n_i$. The results are that $T_i/T_e = 7.8$ at $|X| = 30$–60 R_E, 6.7 at 60–100 R_E, 4.8 at 100–210 R_E, and 5.7 at >210 R_E. Hence there is a tendency for both plasma sheet beta and T_i/T_e to change with distance down the tail in a fashion analogous to that observed for magnetic field strength.

The most significant variations in Figure 8 are those associated with plasma sheet B_z, V_x, and M_A as distance from the earth increases. These parameters all appear to fall into three distance regimes with boundaries at $|X| = 100$ and 210 R_E. We have labeled these three intervals as the near plasma sheet (i.e., $|X| < 100$ R_E), the middle plasma sheet (i.e., $100 < |X| < 210$ R_E), and the distant plasma sheet (i.e., $|X| > 210$ R_E). The near region is characterized on average by strong, >1-nT, positive B_z fields and sub-Alfvénic flow speeds. In the middle region the mean plasma sheet flow becomes strongly tailward, as has been reported by *Zwickl et al.* [1984], and accelerates to super-Alfvénic, $M_A \sim 2$, flow speeds. The B_z magnetic field component is often negative in this region, but the mean field averaged as a function of X remains weakly northward. Finally, there is some continued acceleration with increasing $|X|$ and in the distant plasma sheet the mean flow speeds approach 600 km/s and $M_A \sim 3$. It is in this region that the average plasma sheet field turns negative, $B_z = -0.2$, as was previously reported by *Siscoe et al.* [1984], *Tsurutani et al.* [1984*a*], and *Slavin et al.* [1984*b*].

In Figures 9, 10, and 11, histograms of B_z, V_x, and M_A in the three regions of plasma sheet are displayed. The B_z distribution in Figure 9 starts out predominantly positive in the near plasma sheet (i.e., the solid line). The mean value is $+1.50$ nT, and the standard deviation is 1.26 nT. The distribution for the middle plasma sheet (i.e., the dot-dash line) contains more negative B_z, but the average is still positive, $+0.43$ nT, and the standard deviation remains nearly constant at 1.28 nT. Finally, in the $|X| > 210$ R_E region (i.e., the dashed line) the mean B_z is -0.22 nT, and the standard deviation is 1.29 nT. Thus at all distances down the tail, the B_z distribution retains approximately the same shape and width, but it gradually shifts toward negative values with increasing downstream distance.

Figure 10 displays similar histograms for the X component of flow velocity where negative values correspond to tailward flow. In the near region (i.e., solid line) there is both positive (i.e., earthward) and negative (i.e., tailward) plasma flow. The mean is -106 km/s with a standard deviation of 164 km/s. On the basis of previous investigations [e.g., *Caan et al.*, 1979], we would expect the distribution to be increasingly made up of earthward flow had measurements closer to the earth been included. In addition, the lower average flow

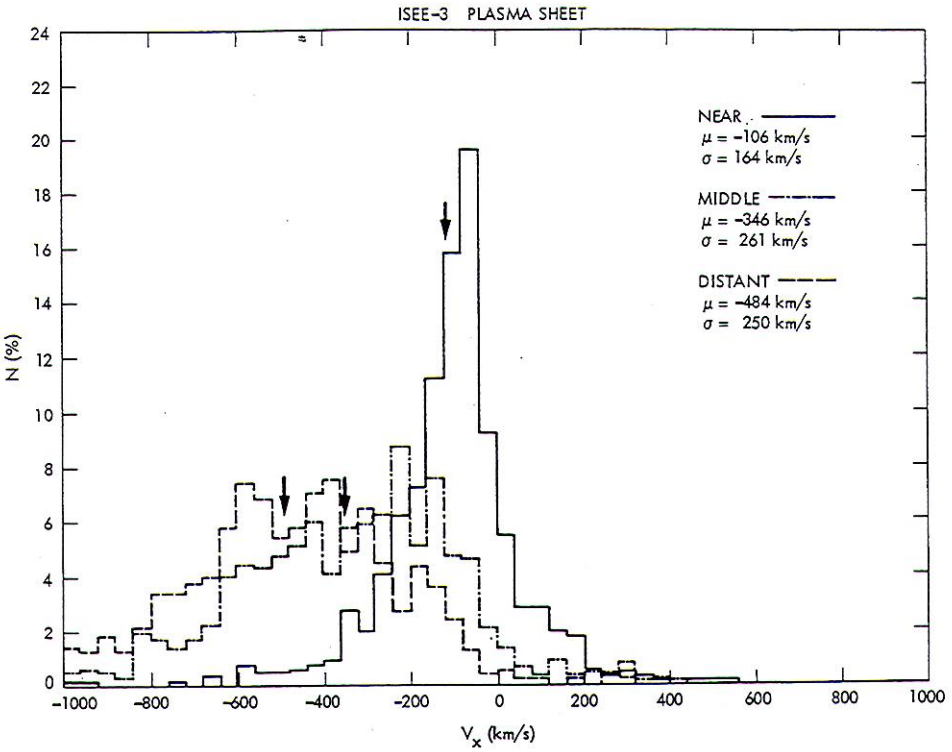

Fig. 10. Histograms of V_x in the plasma sheet are displayed for three distance regimes: near (solid line: $|X| < 100\ R_E$), middle (dot-dash line: $|X| = 100$–$210\ R_E$), and distant (dashed line: $|X| > 210\ R_E$). The means of the three distributions are indicated with dark arrows.

speeds in the cis-lunar plasma sheet are often near or below the limits of reliability for the bulk parameter determinations (*Zwickl et al.* [1984]; see Figure 8). In the middle region (i.e., dot-dash line) the flow is almost entirely tailward with a mean of −346 km/s and standard deviation of 261 km/s. Finally, the distant plasma sheet distribution (i.e., dashed line) exhibits still higher tailward speeds of −484 km/s and a standard deviation of 250 km/s. These results are consistent with those

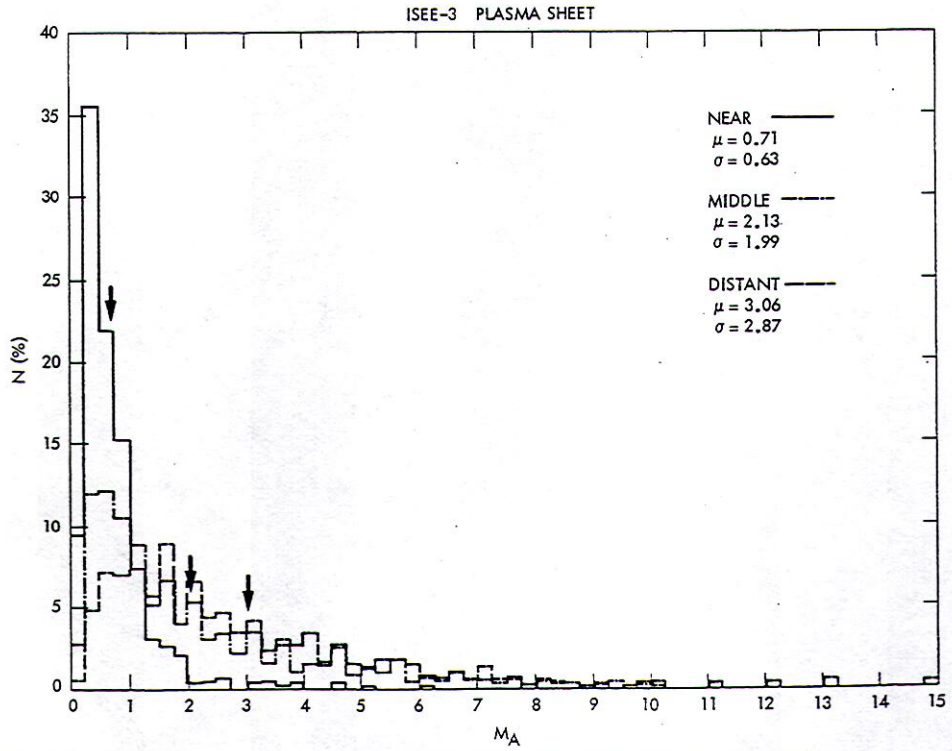

Fig. 11. Histograms of flow speed normalized to the local Alfvén speed are displayed for three distance regimes: near (solid line: $|X| < 100\ R_E$), middle (dot-dash line: $|X| = 100$–$210\ R_E$), and distant ($|X| > 210\ R_E$). The means of the three distributions are indicated with dark arrows.

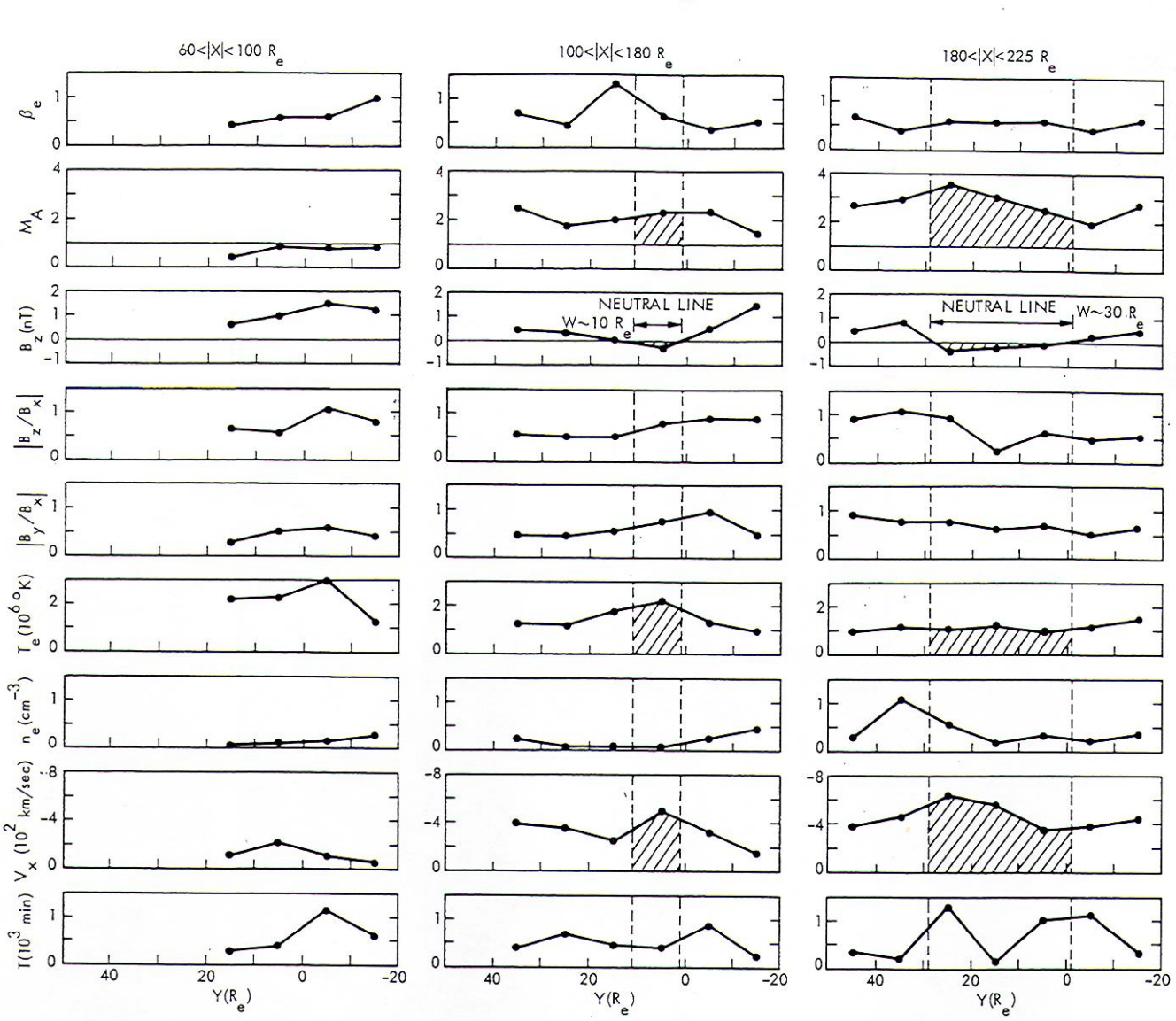

Fig. 12. A set of plasma sheet parameters are plotted versus GSM Y for three distance regimes chosen on the basis of the ISEE 3 trajectory: $|X| = 60$–$100\ R_E$, $|X| = 100$–$180\ R_E$, and $|X| = 180$–$225\ R_E$. Note the appearance of negative B_z in the center of the plasma sheet and the increase in the width of this region between 100–180 R_E and 180–225 R_E. The widths of the corresponding neutral lines are indicated with vertical dashed lines. The regions of negative B_z are accompanied by maxima in electron temperature and flow speed.

of *Zwickl et al.* [1984] and indicate that a major acceleration of the plasma sheet particles takes place between $|X| = 100$ and 200 R_E.

Another important parameter in describing flow conditions in a magnetized plasma is Alfvén Mach number, $V/[B/(4\pi n m_p)^{1/2}]$. Figure 11 displays histograms of M_A in the various regions beginning with the near plasma sheet (i.e., the solid line). As is shown, the M_A distribution at $|X| < 100\ R_E$ is sub-Alfvénic and Gaussian in shape with a mean of 0.71 and a standard deviation of 0.63. The middle region distribution (i.e., dot-dash line) is still largely sub-Alfvénic, but a super-Alfvénic component is present which pulls the mean up to 2.13 with the standard deviation increasing to 1.99. Finally, in the distant plasma sheet (i.e., dashed line) the super-Alfvénic population is dominant and $\langle M_A \rangle = 3.06$ with a standard deviation of 2.87.

These results are quite important because closed magnetic field lines cannot stand in a super-Alfvénic flow (i.e., an "Alfvénic critical point" would form). In the case of the earth the cause of the super-Alfvénic flow is presumably acceleration at a reconnection neutral line(s). The location of the acceleration region is apparently highly variable with intervals of sub-Alfvénic flow being observed out to apogee (see, for example, Figure 11 or examine $|X| = 140$–$150\ R_E$ in Figure 8). However, its average position is probably much closer to $|X| = 100$ than 200 R_E as argued by *Cowley et al.* [1984], *Scholer et al.* [1984*a*], *Zwickl et al.* [1984], *Baker et al.* [1984*b*], and *Daly et al.* [1984*b*].

Having already examined the variation of conditions in the plasma sheet as a function of X, the changes with Y should also be investigated. Figure 12 displays average plasma sheet parameters as a function of GSM Y in three downstream intervals: $|X| = 60$ to 100 R_e, $|X| = 100$ to 180 R_E, and $|X| = 180$ to 225 R_E. These intervals were chosen because

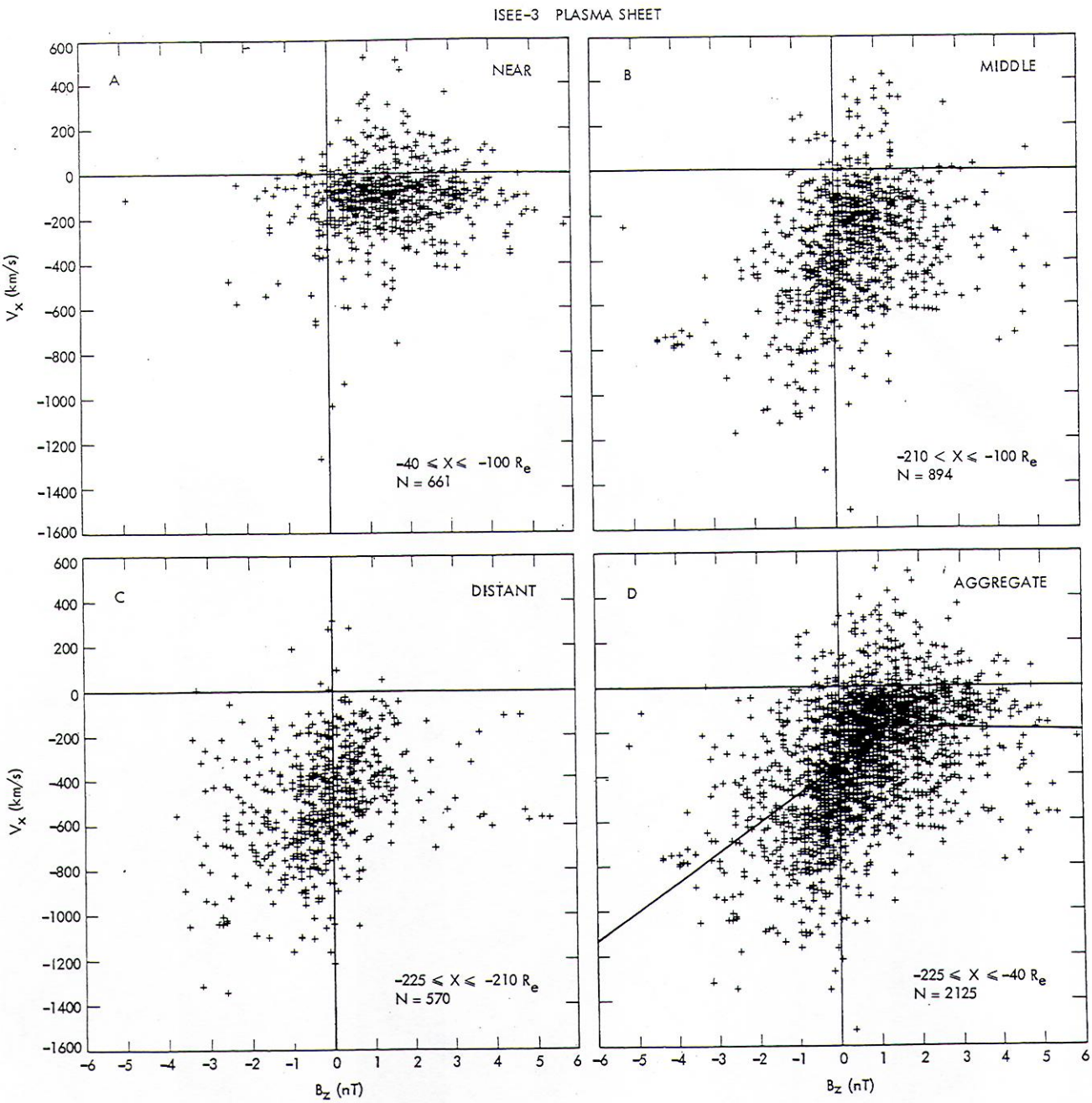

Fig. 13. Plasma sheet V_x is plotted against B_z in GSM coordinates for three different distance regimes: near ($|X| < 100\ R_E$), middle ($|X| = 100$–$210\ R_E$), and distant ($|X| > 210\ R_E$). Negative V_x corresponds to flow away from the earth. Note the strong tendency for high tailward flow speeds to accompany negative B_z. A least squares fit to the aggregate for $B_z < 1$ nT and $B_z > 1$ nT is shown in the final panel.

they represent regions where ISEE 3 moved across the tail and provided the best sampling in $\pm Y$ (see Figure 2). As is shown, at $|X| < 60\ R_E$ the plasma sheet B_z is northward and the flow is sub-Alfvénic. In the $|X| = 100$–$180\ R_E$ region the flow becomes super-Alfvénic as expected from the previous figures. However, by examining plasma sheet conditions as a function of Y it is now clear the B_z also turned negative, but only in a $10\ R_E$ wide region near the aberrated noon-midnight meridian. In this region there is also a maximum in flow speed and electron temperature. At $|X| = 180$–$225\ R_E$ the width of the southward B_z region has grown to $30\ R_E$, and it is still accompanied by maxima in V_x and T_e. Accordingly, the onset of super-Alfvénic flow beyond $|X| = 100\ R_E$ in Figure 8 is indeed accompanied by southward B_z, but the field signature is limited to the central part of the tail. Negative B_z was not visible in the averages in X until the width of the neutral line exceeded half a tail diameter at $|X| > 200\ R_E$. As will be discussed in a later section, the magnetic field results are consistent with the presence of a curved reconnection neutral line in the distant tail and are in qualitative agreement with the results of recent MHD simulations of merging in the magnetotail.

In Figure 13, the reconnection hypothesis is further tested by investigating more closely the relationship between V_x and B_z. Using the 5-min averaged data base, V_x has been plotted against B_z in three distance regimes identified in Figure 8. In

agreement with the previous figures, the GSM Z component of the magnetic field in the plasma sheet at $|X| < 100\ R_E$ was predominantly northward. Reconnection theory would predict earthward flow in this region while the ISEE 3 plasma measurements show slow, tailward flow to be most common. However, it must be noted that the low flow speeds (i.e., <200 km/s) for $B_z > 0$ generally fall into a marginally reliable category determined by Zwickl et al. for plasma parameters derived from the ISEE 3 electron measurements. Furthermore, the plasma sheet flow velocities inferred from the energetic ion anisotropies [*Scholer et al.*, 1984*a*, *b*; *Klecker et al.*, 1984; *Daly et al.*, 1984*b*] do appear to indicate a greater amount of earthward flow at $|X| < 120\ R_E$ than is present in the electron plasma flow determinations [*Zwickl et al.*, 1984]. In addition, Klecker et al. went on to show a strong correlation between tailward (earthward) flow and $B_z < 0$ ($B_z > 0$) when ISEE 3 was near the expected location of the plasma sheet.

In the middle and distant plasma sheet the B_z values are nearly evenly split between positive and negative polarities. For $B_z < 1$ nT there is a good correlation between V_x and B_z, but for $B_z > 1$ nT V_x is independent of B_z. Least squares fits to the aggregate of all the data, $|X| = 40$ to $225\ R_E$, yield

$$\begin{aligned} V_x(\text{km/s}) &= -6.2B_z(\text{nT}) - 162.4 \qquad B_z > 1\ \text{nT} \\ V_x(\text{km/s}) &= 129.7B_z(\text{nT}) - 351.7 \qquad B_z < 1\ \text{nT} \end{aligned} \tag{4}$$

with correlation coefficients of -0.03 and $+0.44$, respectively. The results for $B_z < 0$ agree with the predictions of reconnection theory for a spacecraft tailward of the neutral line and confirm the earlier findings of *Klecker et al.* [1984]. In addition, Figure 13 indicates that for southward B_z the flow speeds are approximately proportional to the magnitude of B_z. The correlation coefficient is not high owing to the large variance in the observations probably associated with plasmoids, convected waves/turbulence, and solar wind perturbations of tail orientation, but there is clear correlation between southward B_z and tailward V_x at the >99% level [*Bevington*, 1969]. Hence given the limitations of the measurements, there appears to be general consistency between the ISEE 3 plasma sheet observations and the predictions of reconnection theory for $B_z < 0$ [e.g., *Nishida and Russell*, 1978]. The lack of earthward flow when B_z is northward may reflect a limitation of the data set or the analyses. However, owing to its critical importance for the various models of the magnetosphere [e.g., *Cowley*, 1982; *Heikkila*, 1984], additional studies, beyond the scope of this investigation, should be undertaken.

SUBSTORM CONDITIONS IN THE LOBE

For the purpose of investigating the effects of substorm activity on the distant tail, a nine-station *AE* index was constructed at the University of Alaska. The time interval covered by the index, days 1–55 of 1983, corresponds approximately to the portion of the ISEE 3 trajectory in Figure 2 with $|X| > 200\ R_E$. The locations of the stations used to create the index are displayed in Figure 14. They are Narssarssuaq (Greenland, geographic east longitude, 314.6°), Abisko (Sweden, 18.8°), Dixon Island (Siberia, 80.6°), Tixie Bay (Siberia, 129.0°), College (Alaska, 211.9°), Yellowknife (Canada, 245.5°), Fort Churchill (Canada, 265.9°), Great Whale River (Canada, 282.2°), and Leirvogur (Iceland, 338.3°). In the standard *AE* index [e.g., *Kamei et al.*, 1983], three additional stations are included: Cape Chelyuskin (Siberia, 104.3°), Cape Wellen (Siberia, 190.2°), and Barrow (Alaska, 203.3°). While the additional three stations would improve the latitudinal coverage of the index, *AE*(9) is expected to be a good proxy for *AE*(12) until the 1983 indices are available. The conditions during the first deep tail pass were moderately disturbed with a mean *AE* of 237 nT for the 55 days considered.

In the cis-lunar magnetotail, substorms are preceded by a buildup in lobe field strength [*Mihalov et al.*, 1968; *Fairfield and Ness*, 1970; *Caan et al.*, 1973; *Slavin and Holzer*, 1979; *Fairfield*, 1979; *Baker et al.*, 1984*a*]. The cause is believed to be enhanced flaring of the magnetopause associated with the addition of magnetic field lines to the tail via reconnection [*Siscoe and Cummings*, 1969; *Coroniti and Kennel*, 1972]. The average distance at which flaring ceases has already been shown to be $|X| = 110$ to $130\ R_E$ in Figure 7. As was discussed by *Slavin et al.* [1983], this result is in good agreement with the analytic flaring-tail model of *Coroniti and Kennel* [1972]. Their model predicts a cessation of flaring at a distance of

$$X^* = X_0 + MR_t[0.6 - \tfrac{1}{3}(R_0/R_t)^3] \tag{5}$$

where X_0 is the inner edge of the tail, typically $10\ R_E$, M is the square root of the ratio of ram pressure to external thermal and magnetic pressure, ~ 7, R_0 is the initial radius of the tail, $\sim 20\ R_E$, and R_t is the terminal radius of the tail, $\sim 30\ R_E$. For these mean parameters the predicted distance where flaring stops is $X^* = 115\ R_E$, in good agreement with our average result. The maximum X^* would be expected to occur during high M conditions (i.e., low dynamic pressure) just before substorm onset when the magnetic flux content of the tail in greatest [*Caan et al.*, 1973; *Slavin and Holzer*, 1979] and the inner edge of the tail is closest to the earth [*Siscoe and Cummings*, 1969]. To approximate these conditions for the purpose of estimating a maximum X^* value, we assume $X_0 = 8\ R_E$, $M = 10$, $R_0 = 20\ R_E$, and $R_t = 35\ R_E$. Under these unusual circumstances, flaring can continue for a time at distances of up to $X^* = 200\ R_E$. However, under more typical conditions, no enhancement in lobe field strength will be expected beyond $|X| = 150\ R_E$. Rather, as the amount of magnetic flux in the magnetotail increases, the cross section of the distant tail simply increases as has been observed [*Maezawa*, 1975; *Baker et al.*, 1984*a*].

Figure 15 investigates the question of distant lobe behavior during substorms directly by plotting magnetic field strength versus *AE*(9) for days 1–55 of 1983 when ISEE 3 was beyond $|X| = 200\ R_E$. Previous studies in the near tail [e.g., *Caan et al.*, 1973] have generally found that lobe field intensity peaks around the time of substorm onset about 15–30 min before the maximum in *AE*. Assuming that magnetic flux addition to the tail takes place at the solar wind speed, an additional delay at ISEE 3 of 30–45 min is anticipated. Therefore a number of different time lags between 0 and 90 min were tried with the 30- and 45-min lags in Figure 15 being representative examples. In all cases the strength of the magnetic field in the distant lobes was approximately 1 nT weaker for $AE < 200$ nT than for $AE > 200$ nT. However, for $AE > 200$ nT the actual strength of the field was independent of the level of substorm activity measured by *AE*. In the absence of a positive correlation between B and *AE* during moderate to strong substorms (i.e., $AE > 200$ nT), we attribute the slightly weaker lobe fields during intervals of very low *AE* to a secondary correlation between *AE* and V, B, and nV^2 in the solar wind [e.g., *Garrett et al.*, 1974]. High values of solar wind pressure will produce greater lobe field intensities without needing to invoke any significant magnetopause flaring beyond $200\ R_E$. A definitive demonstration that substorm-associated flaring of

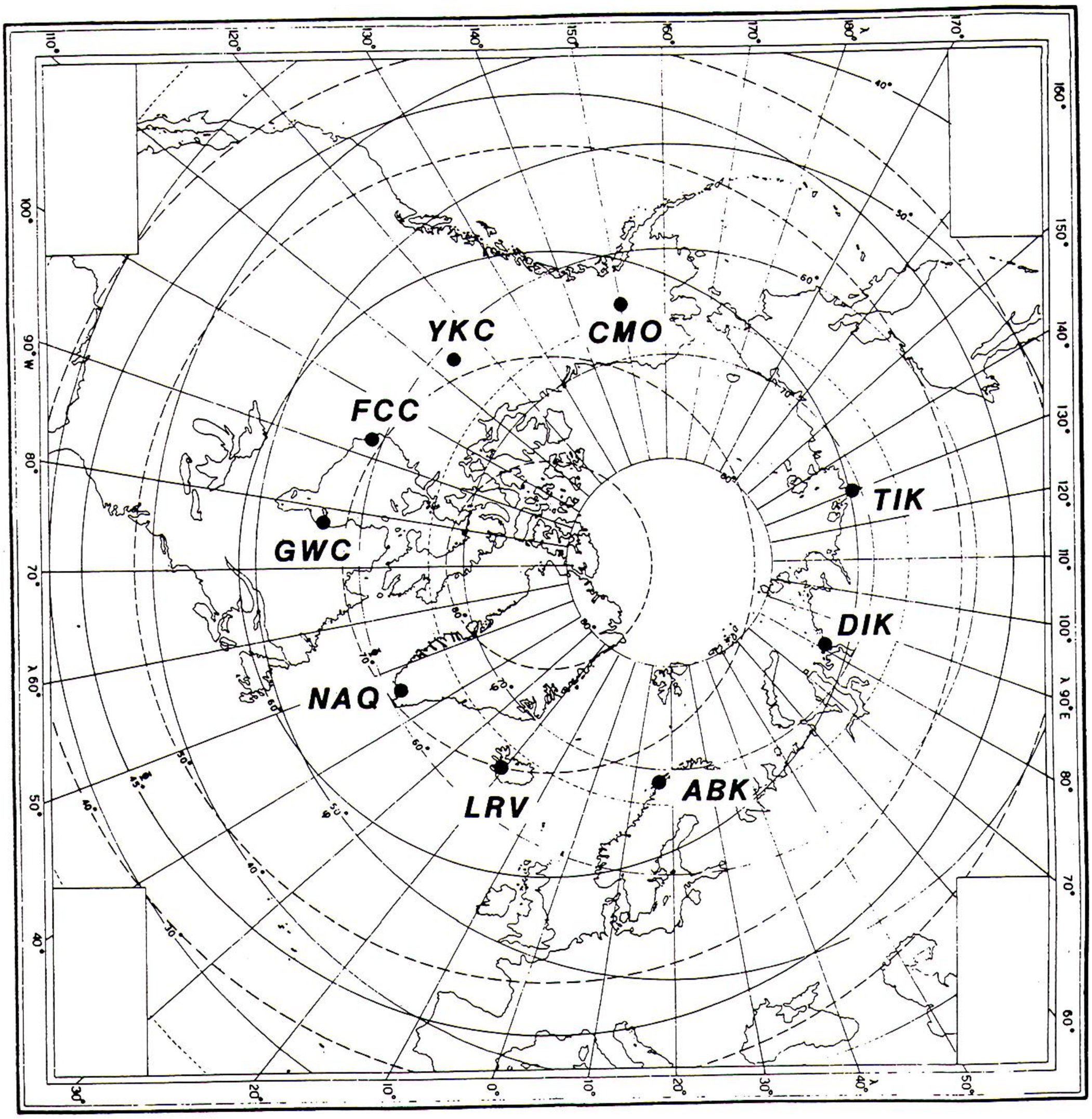

Fig. 14. The geographic (solid grid) and geomagnetic (dashed grid) positions of the nine stations utilized to produce the *AE* used in this study are displayed.

the magnetopause does not occur in the distant tail will require the use of upstream solar wind measurements to scale the ISEE 3 lobe magnitudes to a single external pressure prior to comparison with *AE*. This procedure would remove the secondary correlations, but it falls outside the scope of this study and will be examined at a later time.

In addition to lobe field strength we have also correlated *AE* and other lobe parameters with similar negative results. Figure 16 displays the results for electron beta and Alfvénic Mach number. Owing to the interrelationships between magnetopause reconnection, the entry of plasma into the magnetosphere, and the magnetospheric convection electric field, some correlation between lobe β_e, M_A, and *AE* might have been expected. However, as is shown in Figure 16, lobe Mach number is independent of *AE* and electron beta shows only a weak negative correlation. Hence we conclude that large-scale conditions in the lobes at $|X| > 200\ R_E$ are at best only weakly influenced by the effects of substorms and flaring. Short-scale length phenomena, such as traveling compression regions [*Slavin et al.*, 1984*a*], would not be resolved in the surveys conducted in Figures 15 and 16.

Substorm Conditions in the Plasma Sheet

A fundamental prediction of the reconnection-based models of substorm activity is that following the expansion phase southward magnetic fields will be observed embedded in high-speed flows away from the earth in the distant tail [*Dungey*, 1961; *McPherron et al.*, 1973]. Searches for such signatures in

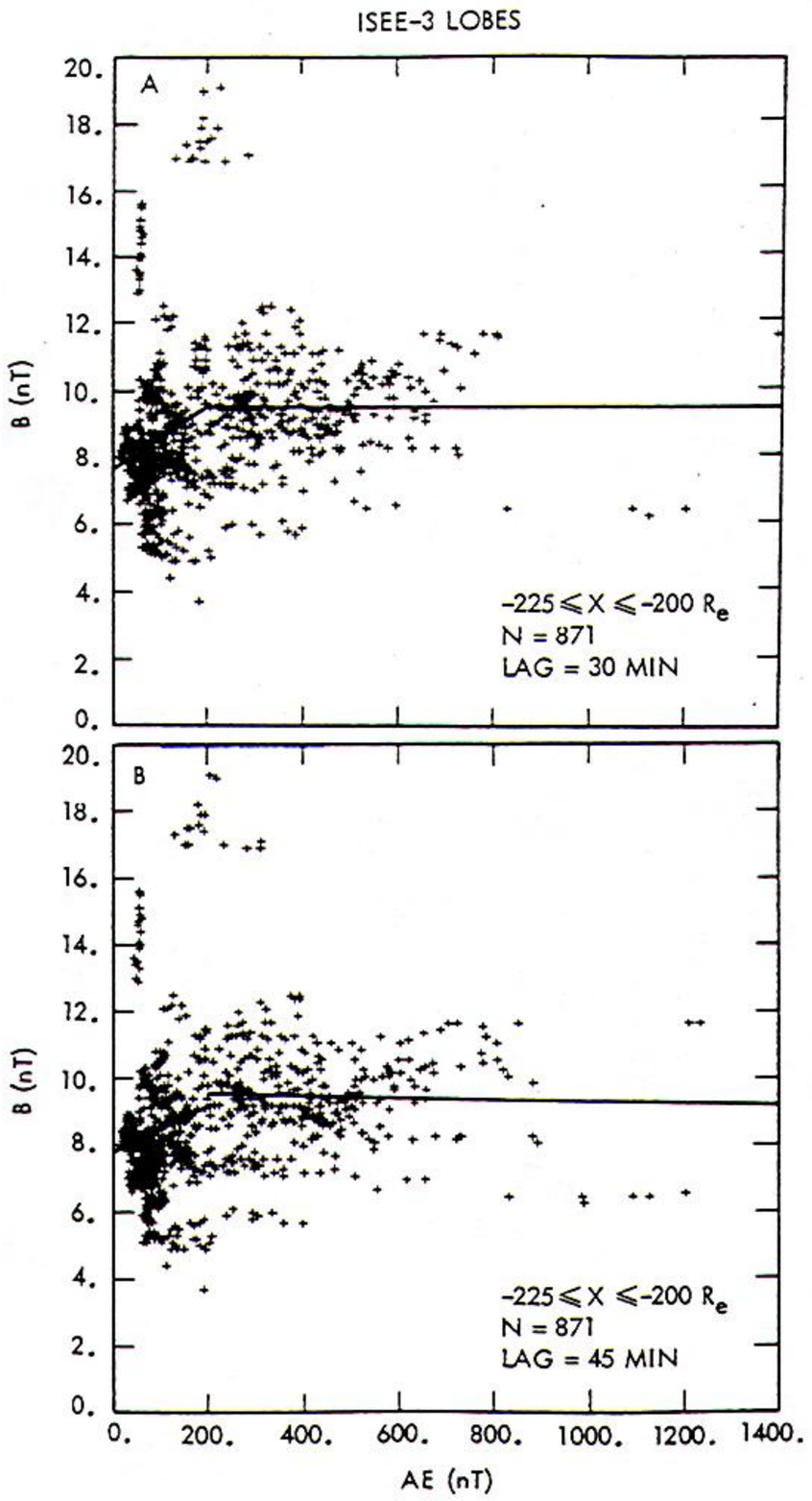

Fig. 15. The lobe magnetic field strength at $|X| > 200\ R_E$ is plotted versus $AE(9)$ for time lags of 30 and 45 min. The least squares fits for $AE < 200$ nT and $AE > 200$ nT are displayed.

the cis-lunar tail have produced mixed results [e.g., *Lui et al.*, 1977; *Caan et al.*, 1979]. However, in general, some southward shift in the B_z distribution is observed in the tailward flows as contrasted with the earthward flows [*Nishida and Nagayama*, 1973; *Caan et al.*, 1979; *Nishida et al.*, 1981; *Hayakawa et al.*, 1982]. The ISEE 3 observations offer far better opportunities than the earlier missions for the study of conditions tailward of the neutral line because of the large amount of time it spends in the distant tail. Some observation of the tailward region is possible when near-earth neutral lines form during substorms, but Figure 8 suggests that continuous observation of this region requires the spacecraft to be located more than 100–200 R_E downstream of the earth.

The entry of ISEE 3 into the plasma sheet often coincides with the passage of plasmoids down the tail [*Hones et al.*, 1984*a*; *Baker et al.*, 1984*a*]. Plasmoids are large magnetic islands believed to form in the plasma sheet as a result of rapid reconnection at $X = -15$ to $-40\ R_E$ [*Schindler*, 1974; *Hones*, 1979; *Birn and Hones*, 1981; *Lee et al.*, 1985]. These topologically distinct structures move rapidly downstream and are observed by spacecraft as rotations of the magnetic field in conjunction with high-speed flows. Studies of plasmoids in the ISEE 3 apogee observations have found them to occur usually about 30 min following the onset of substorm activity at geosynchronous orbit and in ground-based magnetograms [*Hones et al.*, 1984*a*; *Baker et al.*, 1984*a*]. While plasmoids transport no net north-south magnetic flux down the tail, they do produce strong $\pm B_z$ fields in the plasma sheet. In addition, simulation studies indicate that the plasma flows associated with plasmoid creation are not one dimensional and can be quite complex [*Birn and Hones*, 1981; *Lee et al.*, 1985]. Hence plasmoids will introduce significant amounts of "noise" into all correlations involving the B_z magnetic field component.

With these caveats in mind, Figure 17 plots 5-min averaged B_z and V_x against $AE(9)$. Despite the presence of considerable variance, possibly associated in part with plasmoids, the magnetic field becomes increasingly southward and the flow speed more negative as the level of substorm activity increases. Quiet AE levels, <100 nT, correspond to slightly northward mean B_z and tailward flow speeds of 0 to 300 km/s. In contrast, for very intense substorms, $AE > 1000$ nT, the mean B_z approaches -2 nT and $V_x = -1000$ km/s. The linear least squares regressions displayed in Figure 17 are

$$B_z = -1.84 \times 10^{-3}\ AE + 0.43$$
$$V_x = -0.44\ AE - 346.2 \tag{6}$$

with correlation coefficients of -0.32 and -0.35, respectively. Figure 18 takes the examination of plasma sheet conditions a step farther by plotting electron beta and Alfvén Mach

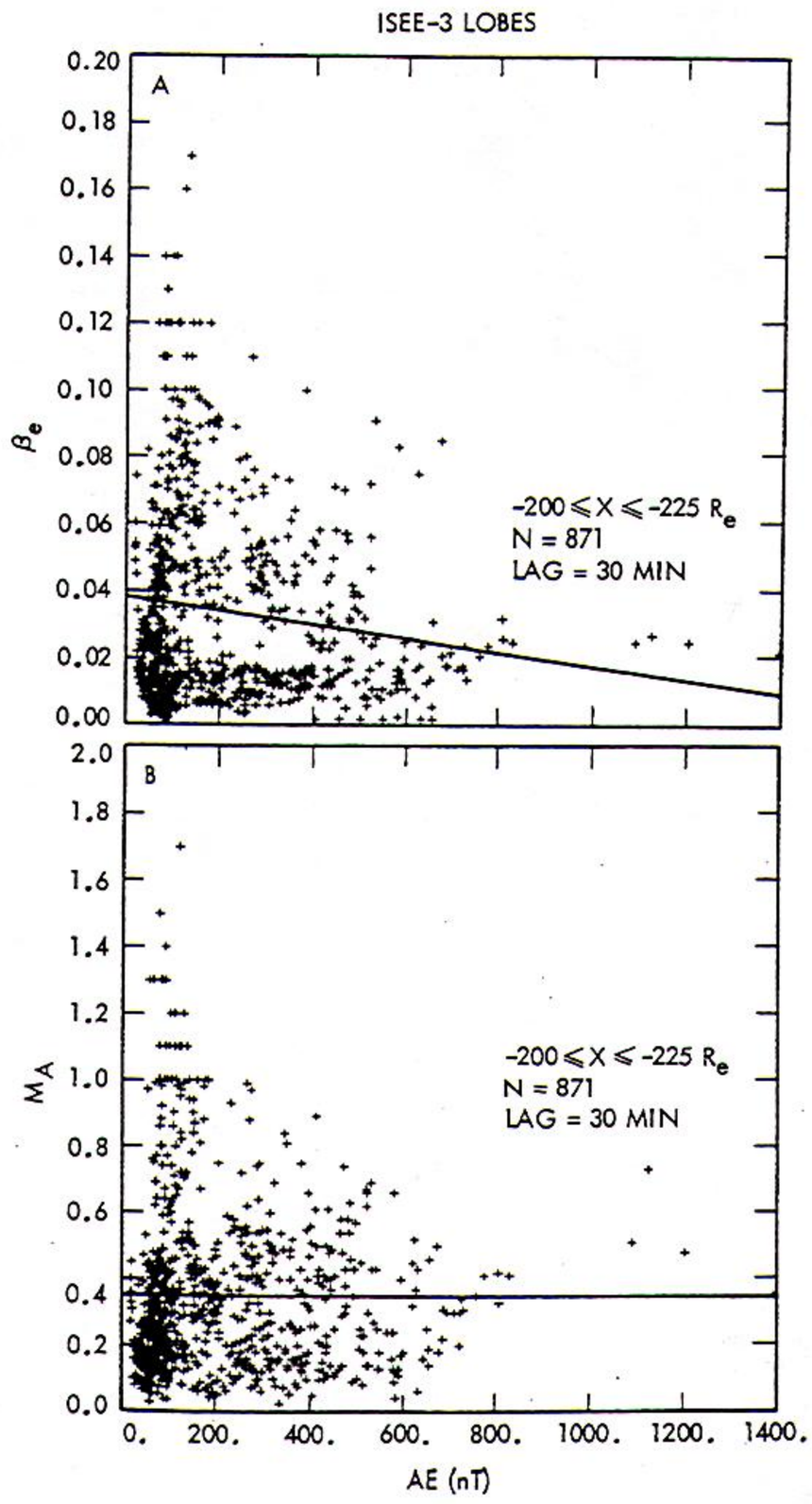

Fig. 16. Lobe electron beta and flow speed normalized to the local Alfvén Mach number at $|X| > 200\ R_E$ are plotted against $AE(9)$ with 30-min time lags. As shown, these quantities do not appear to be strongly correlated with AE.

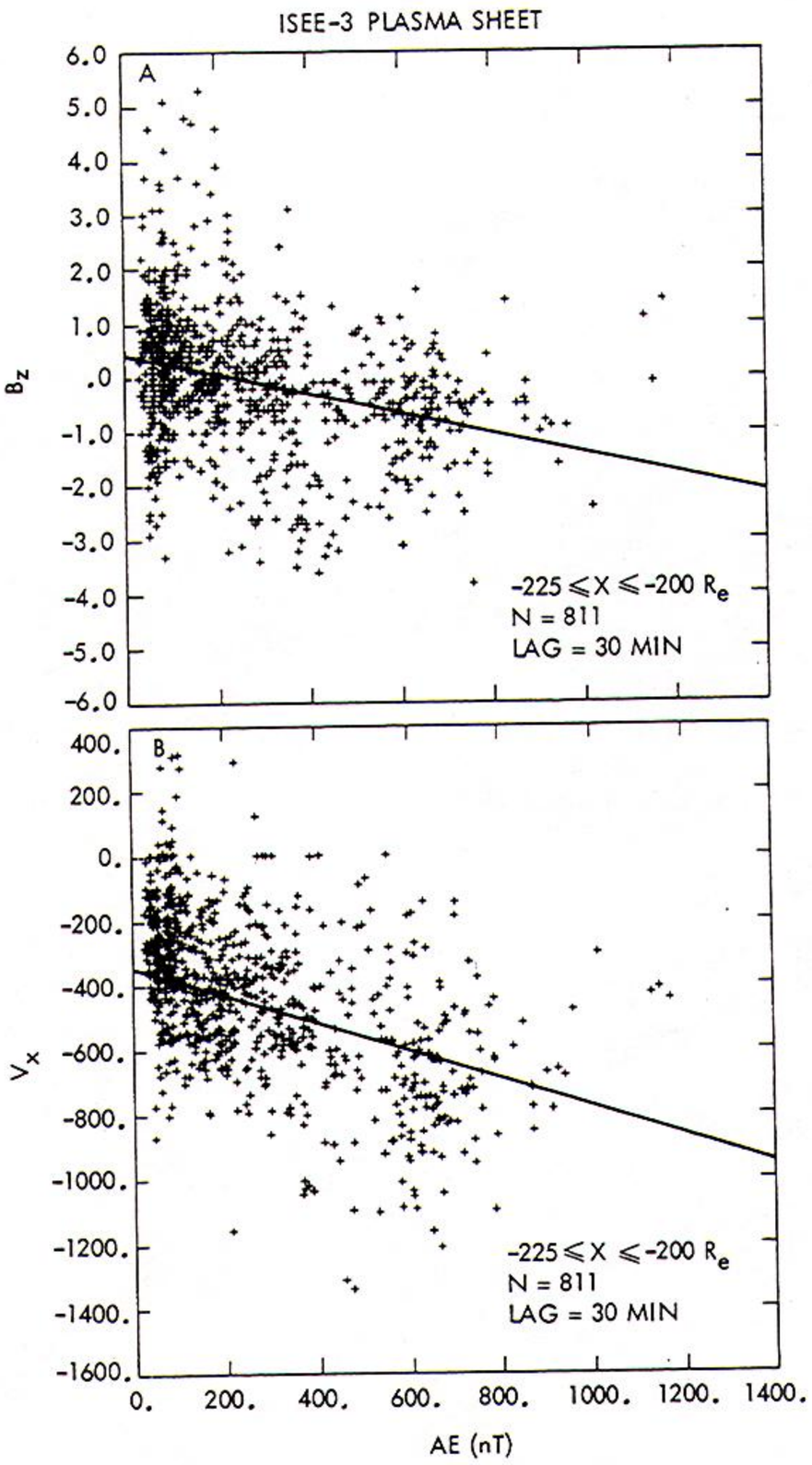

Fig. 17. Plasma sheet B_z and V_x are plotted against $AE(9)$ with a 30-min time lag. As shown, both quantities are well correlated with substorm activity as predicted by the reconnection-based models of the substorm process.

number versus AE. As is shown, the correlations between AE and these two parameters are weak or absent, but M_A does tend to increase with the level of substorm intensity. Hence the ISEE 3 distant tail plasma sheet observations do show clear substorm effects with respect to the critical B_z and V_x parameters. Their sense, more negative B_z and tailward V_x with increasing levels of substorm activity, is in agreement with the predictions of the reconnection-based models of the substorm process.

DISCUSSION

The east-west tail diameter of 60 ± 5 R_E determined by this study in Figures 2 and 3 is in good agreement with the initial survey of *Slavin et al.* [1983]. Furthermore, it has been shown that a distant tail diameter of 60 R_E is consistent with the flaring tail models of magnetopause geometry and previous estimates of tail dimensions made closer to earth. However, it exceeds by 30% the 45 R_E east-west tail width reported by *Tsurutani et al.* [1984*b*]. The reason for this discrepancy appears to be that their analysis was based upon lists of tail lobe and plasma sheet intervals which excluded boundary layers and hence did not map out the full extent of the tail. More detailed studies of tail dimensions using interplanetary and ground-based observations to correct for changing solar wind flow direction, external pressure, and tail magnetic flux content [cf. *Maezawa*, 1975; *Baker et al.*, 1984*a*] should also be performed. However, they fall outside the scope of this investigation and will be pursued in a later study.

The presence of plasma in the lobes of the magnetotail was well known from earlier missions [e.g., *Hardy et al.*, 1979]. The solar wind is thought to be the dominant source of these "mantle" particles which $E \times B$ drift from the outer lobes toward the plasma sheet. The important contribution of ISEE 3 is the observation of how lobe plasma density varies with distance down the tail and east-west location within the lobes. *Pilipp and Morfill* [1978] have investigated lobe plasma conditions using models in which solar wind plasma enters either only at the cusp or continuously along the tail magnetopause. As is shown in the top panels of Figure 19, the cusp entry model produces nonmonotonic X and Z gradients with most of the plasma particles following similar trajectories determined by the mean tailward velocity of the initial distribution. The model calculations are two dimensional so that Z is actually distance toward the magnetopause, and hence it generally corresponds to Y along the ISEE 3 trajectory in Figure 2. In order to get the strong density and weak velocity gradients in X and Y found by this study, the Pilipp and Morfill calculations in the lower panel of Figure 19 show that a continuous entry of particles down the length of the tail magnetopause is

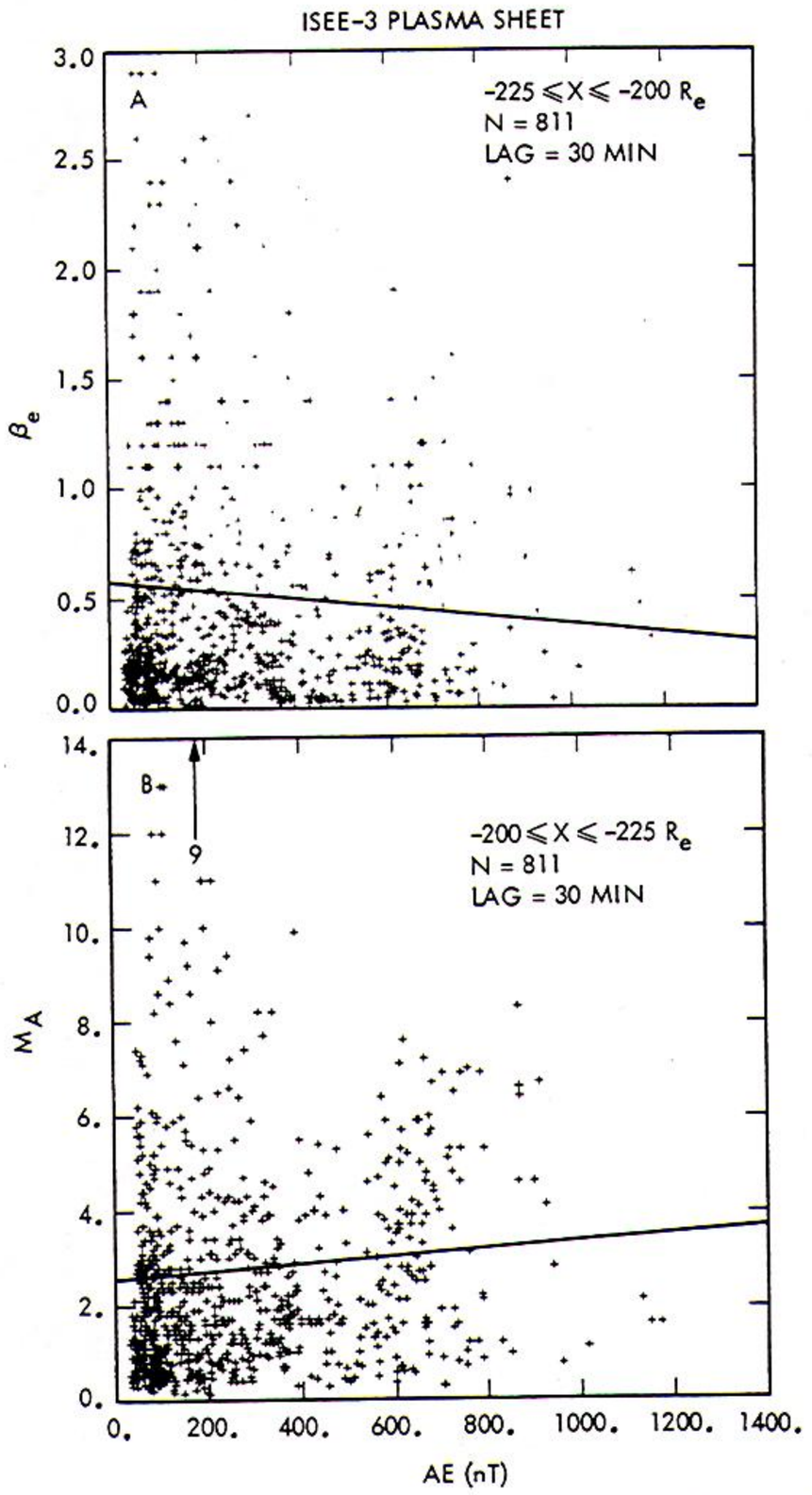

Fig. 18. Plasma sheet electron beta and flow speed normalized to the local Alfvén speed are plotted versus $AE(9)$ with a 30-min time delay. Neither quantity appears to be strongly correlated with AE.

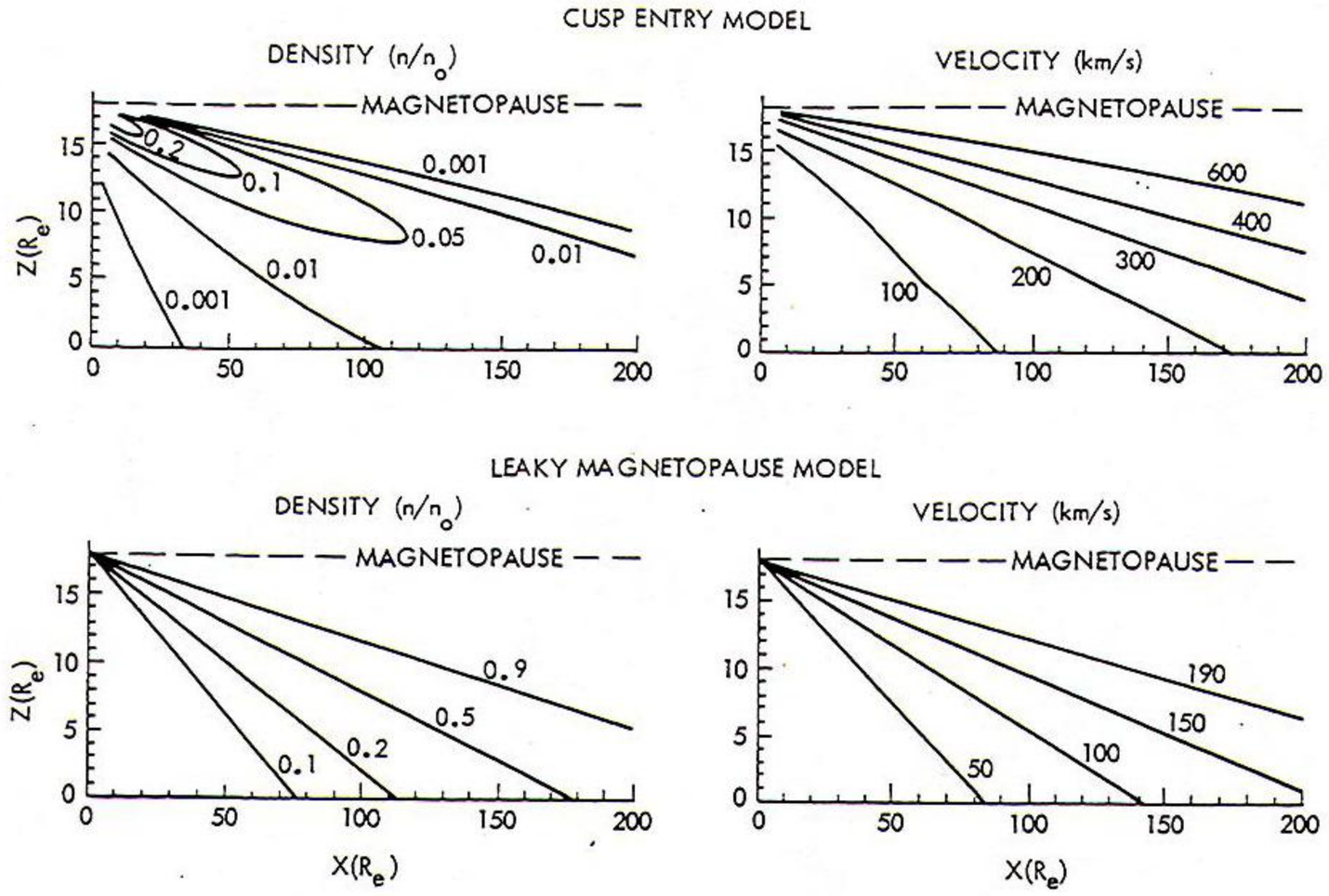

Fig. 19. Lobe velocity and density profiles from the *Pilipp and Morfill* [1978] cusp entry and leaky magnetopause mantle models are displayed. The strong density and weak velocity gradients in $|X|$ and $|Y|$ appear better represented by the leaky magnetopause model.

necessary. Otherwise the "velocity filter" effect will cause a rapid increase in tailward flow speed with increasing $|X|$ and $|Y|$, and insufficient plasma will be available for any significant filling of the lobes. The agreement between the "leaky magnetopause" model of Pilipp and Morfill and the X and Y lobe gradients in V_x and n displayed in Figures 4 and 6 is reasonably good. Accordingly, the ISEE 3 distant tail observations appear to require a small, but continuous entry of solar wind particles across the downstream magnetopause. The sites for solar wind particle entry are probably "patches" or "windows" on the magnetopause [*Stern*, 1973; *Sibeck et al.*, 1985*a*, *b*] where magnetic flux is being added to the tail and significant magnetic fields normal to the magnetopause surface are present. Finally, as is discussed by *Sibeck et al.* [1985*b*], the anticorrelation between n and $|B_y/B_x|$, $|B_z/B_x|$ as ISEE 3 moved from the central lobes toward the magnetopause is also consistent with the slow expansion fan models of the plasma mantle–magnetosheath interface [*Levy et al.*, 1964; *Coroniti and Kennel*, 1979; *Swift and Lee*, 1983].

Perhaps the major prediction of the open model of the magnetosphere is that there always will be at least one reconnection neutral line within the magnetotail [*Dungey*, 1961; *Russell and McPherron*, 1973; *Cowley*, 1980]. During substorm intervals when plasmoids are formed there may in fact be a number of X and O type neutral lines produced which later move downstream leaving a single quasi-stationary neutral line in the distant tail until the next substorm [e.g., *Birn and Hones*, 1981; *Lee et al.*, 1985]. The classical signatures expected tailward of the neutral line are high-speed flow away from the earth with embedded southward magnetic fields.

The fast, predominantly tailward flows evident in Figure 8 beginning around $|X| = 100\ R_E$ have been reported by previous studies [*Cowley et al.*, 1984; *Scholer et al.*, 1984*a*; *Zwickl et al.*, 1984; *Daly et al.*, 1984*b*] and were used to argue that the mean location of the distant neutral line is about 100 R_E downstream of the earth. In this study we have gone on to show that the flow speeds in the distant plasma sheet are also super-Alfvénic and their values are well-correlated southward B_z. The magnitude of the flow speed out of the diffusion region where the field lines actually merge is only loosely constrained on theoretical grounds by geometry and conservation of mass in the Petschek-type slow shock merging models [*Petschek*, 1964; *Vasyliunas*, 1975]. However, $M_A \simeq$ 1–2 flows, such as those found by this study, have been produced in MHD simulations of merging in the tail [*Sato et al.*, 1984]. Accordingly, both the direction and magnitude of the flows measured by ISEE 3 in the distant plasma sheet are consistent with reconnection near the east-west center of the magnetotail.

However, as has been pointed out by *Zwickl et al.* [1984] and *Daly et al.* [1984*b*], a simple neutral line stretching across the tail near $|X| = 100\ R_E$ is not consistent with the ISEE 3 average magnetic field results [*Siscoe et al.*, 1984; *Tsurutani et al.*, 1984*a*; *Slavin et al.*, 1984*b*]. As is shown in Figure 8, the Z component of the plasma sheet magnetic field averaged as a function of X does not turn southward until $|X| = 210\ R_E$, or about 100 R_E farther downstream than where the flow became tailward and super-Alfvénic. Conservation of magnetic flux arguments may be used to show that reconnection will result in average plasma sheet B_z values of -0.1 to -0.3 nT [*Slavin et al.* 1984*b*]. However, the presence of plasmoids [*Hones et al.*, 1984*a*] and reconnection-generated turbulence [*Coroniti et al.*, 1978] results in very broad B_z distributions (i.e., standard deviation of >1 nT) as displayed in Figure 9. It was on this basis that *Slavin et al.* [1984*b*] pointed out that reconnection will never make the plasma sheet B_z field negative more than slightly over half of the time as observed for $|X| > 210\ R_E$ in Figure 9.

In this study we have contributed to the resolution of the neutral line location problem by examining plasma sheet parameters as a function of Y as well as X. The results in Figure 12 show, contrary to the findings of the previous studies which only considered evolution along the X axis, that B_z does indeed turn southward near the distance where the flow becomes super-Alfvénic. However, the region of southward B_z at $|X| = 100$–$180\ R_E$ is only 10 R_E wide and located near the

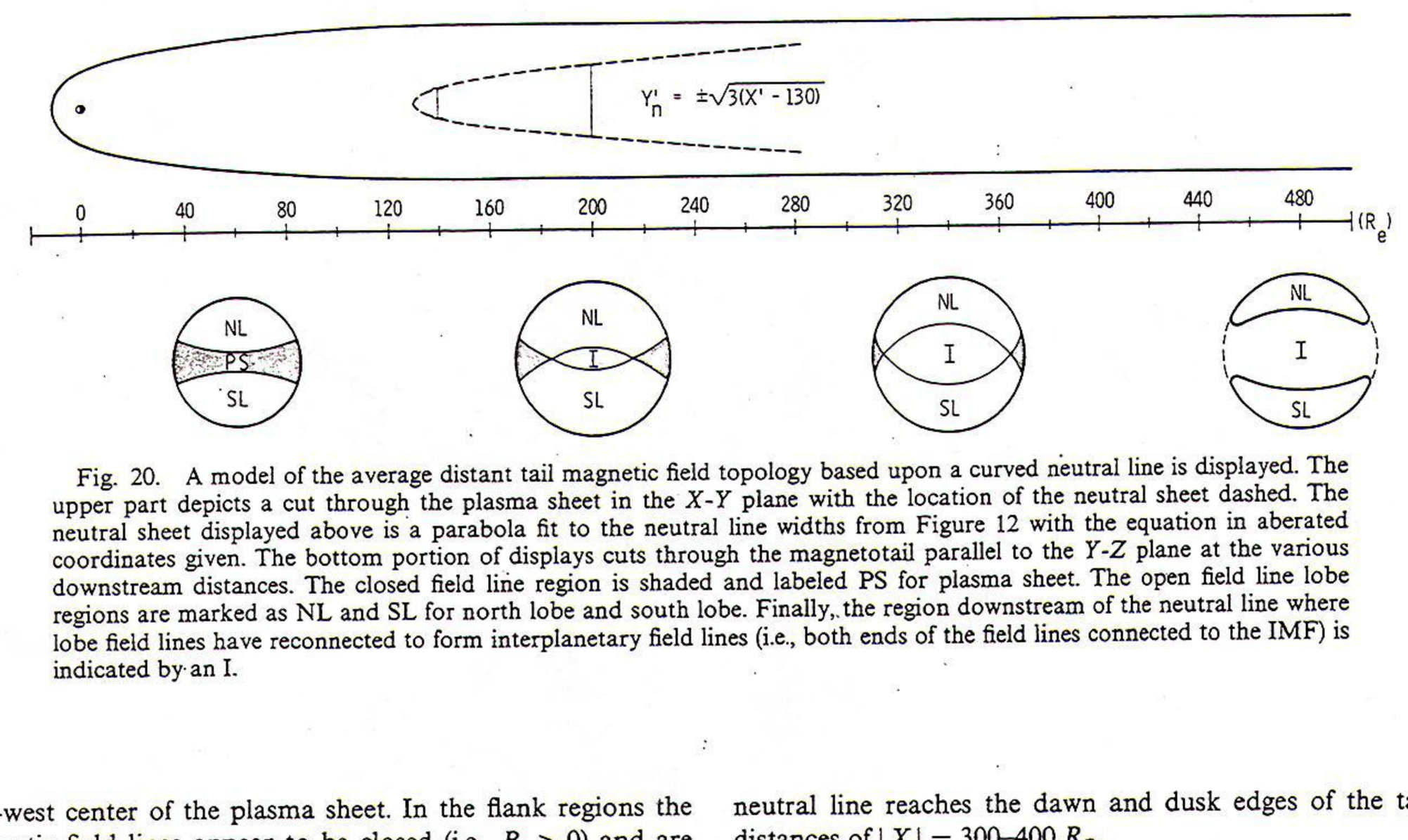

Fig. 20. A model of the average distant tail magnetic field topology based upon a curved neutral line is displayed. The upper part depicts a cut through the plasma sheet in the X-Y plane with the location of the neutral sheet dashed. The neutral sheet displayed above is a parabola fit to the neutral line widths from Figure 12 with the equation in aberated coordinates given. The bottom portion of displays cuts through the magnetotail parallel to the Y-Z plane at the various downstream distances. The closed field line region is shaded and labeled PS for plasma sheet. The open field line lobe regions are marked as NL and SL for north lobe and south lobe. Finally, the region downstream of the neutral line where lobe field lines have reconnected to form interplanetary field lines (i.e., both ends of the field lines connected to the IMF) is indicated by an I.

east-west center of the plasma sheet. In the flank regions the magnetic field lines appear to be closed (i.e., $B_z > 0$) and are still being swept tailward. At $|X| = 180$–225 R_E the width of the negative B_z region grows to 30 R_E. The magnitude of the southward B_z, -0.1 to -0.3 nT, is consistent with reconnection as discussed earlier, and these regions of $B_z < 0$ also correspond to maxima in plasma flow speed and electron temperature. The reasons for reconnection taking place preferentially near the east-west center of the tail are not clear, but recent MHD simulations [*Birn and Hones*, 1981] have found this to be the case owing to the plasma sheet being thinnest near the center of the tail. Clearly, additional ISEE 3 data analysis and three-dimensional theoretical modeling will be needed before these potentially important new results are understood.

In Figure 20 we present a three-dimensional model of tail magnetic topology which is consistent with the magnetometer observations presented in this study. The top half of the figure displays, looking down from the north, a planar cut through the plasma sheet in the X-Y plane. The neutral line which fits the B_z observations is shown by a dashed line. It is found nearest to the earth near the east-west center of the tail where its average position is $|X| = 120$–140 R_E. The closeness of the ISEE 3 trajectory to the location of the neutral sheet while at $|X| \triangleq 100$–200 R_E is also consistent with the observations of reconnection-associated slow shocks [*Feldman et al.*, 1984; *Smith et al.*, 1984] and neutral line crossings [*Baker et al.*, 1984*b*] at these distances.

In this model the neutral line is curved and lies farther from the earth as one moves toward dawn or dusk. Given only the ISEE 3 measurement of the reconnection line width at two distances, $|X| = 100$–180 and 180–225 R_E, the selection of a parabola (equation given in the figure) to fit the observations is not unique, but the fit is reasonably good and consistent with the observations. The idea of a curved neutral line in the distant tail originated with *Russell* [1977] in the course of interpreting energetic particle observations made from lunar orbit [*Lin et al.*, 1977]. The reason for the curve in the neutral line is not clear, but Russell suggested that it might be related to the viscous component of the solar wind–magnetosphere interaction and the stresses it places on the tail. Depending upon the choice of curve to fit the ISEE 3 observations, the neutral line reaches the dawn and dusk edges of the tail at distances of $|X| = 300$–400 R_E.

The bottom half of Figure 20 shows transverse cuts through the magnetotail parallel to the Y-Z plane at various downstream distances. Labels and shading are used to indicate the magnetic field line topology in each region. The plasma sheet is generally believed to reside on closed field lines with both feet on the earth [*Crooker*, 1977]. It corresponds to the shaded regions in the figure. The north and south lobe regions, NL and SL, are composed of open field lines with one foot on the earth and the other end connected to the interplanetary magnetic field. Reconnection in the tail creates closed field lines in the region earthward of the neutral line and interplanetary field lines on the tailward side. Accordingly, a curved neutral line would be expected to produce a region of interplanetary field lines (i.e., no feet on the earth) in the center of the tail which grows at the expense of the plasma sheet and lobe regions with increasing $|X|$. In the ISEE 3 observations, which were largely confined to the vicinity of the X-Y plane, the corresponding quasi-two-dimensional signature of the curved neutral line is an increase in the east-west extent of the region where $B_z < 0$ as distance down the tail increases. Eventually, only small north and south lobe regions remain with a thick region of interplanetary field (plus plasmoids and other magnetospheric debris) separating them.

SUMMARY

In this study, both average and substorm conditions in the distant magnetotail have been investigated using ISEE 3 magnetic field and plasma observations. The diameter of the tail, the strength of the lobe magnetic fields, and their dependence upon downstream distance were all found to agree well with the flaring tail models of magnetopause geometry and pressure balance [*Spreiter and Alksne*, 1969; *Coroniti and Kennel*, 1972; *Birn et al.*, 1977]. The gradual filling of the lobes by mantle plasma reported in previous ISEE 3 studies [*Bame et al.*, 1983; *Zwickl et al.*, 1984; *Gosling et al.*, 1984; *Sibeck et al.*, 1985*b*] has been further investigated. The results were found to be in qualitative agreement with the leaky magnetopause model of *Pilipp and Morfill* [1978] which requires continuous solar wind particle entry over the entire length of the mag-

netopause. Large-scale conditions in the distant, $|X| > 200$ R_E, lobes were examined as a function of substorm activity. Little or no correlation was found between lobe parameters and AE.

In the plasma sheet the variations in plasma parameters with X, $\pm Y$, and AE have been examined. The most important results concern the existence of reconnection and the location and shape of the neutral line. At all distances the greatest tailward flow speeds were shown to be directly proportional to the embedded southward B_z. It was also found that the magnitudes of tailward V_x and southward B_z are directly proportional to the level of substorm activity near the earth as measured by the AE index. These reconnection signatures have long been sought in the near-earth magnetotail [e.g., *Russell and McPherron*, 1973; *Lui et al.*, 1977; *Nishida and Russell*, 1978] but were never observed as unambiguously as in the ISEE 3 distant tail measurements. As a function of X the average flow becomes super-Alfvénic and tailward just beyond $|X| = 100$ R_E. The $M_A = 1$–3 flow speeds are in good agreement with the predictions of recent MHD simulations of magnetotail reconnection [*Sato et al.*, 1984]. The average plasma sheet B_z also turns southward near that distance but only in a 10 R_E wide region centered on the aberrated X axis. MHD simulations using realistic plasma sheet geometries which are thinnest near the aberrated noon-midnight meridian have predicted that reconnection will preferentially occur near the center of the tail but with the flow signature spread over a greater distance in Y than the B_z signature [*Birn and Hones*, 1981]. The observation of tailward flow and northward B_z on the dawn and dusk sides of the plasma sheet suggests that closed field lines are still being dragged tailward, perhaps by the viscous component of the solar wind–magnetosphere interaction along the flanks at $|X| = 200$ R_E. The width of the region of negative B_z increases with downstream distance and reaches 30 R_E at $|X| = 200$ R_E. We have interpreted this finding as strong evidence for a curved distant neutral line which is closest to the earth near local midnight and curves away from the earth toward the dawn and dusk sides of the tail. The existence of such a curved neutral line sheet was suggested some time ago by *Russell* [1977], and our results appear to support his hypothesis. Accordingly, the results of this investigation may require global three-dimensional MHD models of the magnetotail before their implications can be fully understood.

Acknowledgments. The authors wish to thank J. E. Wolf for assistance with computational aspects of the data analysis. The authors also wish to acknowledge useful discussions of this study with J. T. Gosling, J. Birn, and W. Heikkila. The research contained in this report was carried out at the Jet Propulsion Laboratory, California Institute of Technology, under contract to the National Aeronautics and Space Administration. The work at Los Alamos was performed under the auspices of the U.S. Department of Energy with support from NASA.

The Editor thanks A. Nishida and D. A. Hardy for their assistance in evaluating this paper.

REFERENCES

Atkinson, G., A theory of polar substorms, *J. Geophys. Res.*, *71*, 5157, 1966.

Axford, W. I., and C. O. Hines, A unifying theory of high latitude geophysical phenomena and geomagnetic storms, *Can. J. Phys.*, *3*, 1433, 1961.

Baker, D. N., S. J. Bame, R. D. Belian, W. C. Feldman, J. T. Gosling, P. R. Higbie, E. W. Hones, Jr., D. J. McComas, and R. D. Zwickl, Correlated dynamical changes in the near earth and distant magnetotail regions: ISEE 3, *J. Geophys. Res.*, *89*, 3855, 1984*a*.

Baker, D. N., S. J. Bame, J. Birn, W. C. Feldman, J. T. Gosling, E. W. Hones, Jr., R. D. Zwickl, J. A. Slavin, E. J. Smith, B. T. Tsurutani, and D. G. Sibeck, Direct observations of passages of the distant line (80–140 R_e) following substorm onsets, *Geophys. Res. Lett.*, *11*, 1042, 1984*b*.

Bame, S. J., J. R. Asbridge, H. E. Felthauser, J. P. Glore, H. L. Hawk, and J. Chavez, ISEE-C solar wind plasma experiment, *IEEE Trans. Geosci. Electr.*, *GE-16*, 160, 1978.

Bame, S. J., R. C. Anderson, J. R. Asbridge, D. N. Baker, W. C. Feldman, J. T. Gosling, E. W. Hones, Jr., D. J. McComas, and R. D. Zwickl, Plasma regimes in the deep geomagnetic tail: ISEE-3, *Geophys. Res. Lett.*, *10*, 912, 1983.

Bavassano, B., F. Mariani, and U. Villante, Far magnetospheric field observations by Pioneer 8: The distant bow shock and extended tail, *Space Res.*, *14*, 403, 1974.

Behannon, K. W., Mapping the earth's bow shock and magnetic tail by Explorer 33, *J. Geophys. Res.*, *73*, 907, 1968.

Bevington, P. R., *Data Reduction and Error Analysis for the Physical Sciences*, McGraw-Hill, New York, 1969.

Bieber, J. W., E. C. Stone, E. W. Hones, Jr., D. N. Baker, S. J. Bame, and R. P. Lepping, Microstructure of magnetic reconnection in the earth's magnetotail, *J. Geophys. Res.*, *89*, 6705, 1984.

Birn, J., and E. W. Hones, Jr., Three-dimensional computer modeling of dynamic reconnection in the geomagnetic tail, *J. Geophys. Res.*, *86*, 6802, 1981.

Birn, J., R. R. Sommer, and K. Schindler, Self-consistent theory of the quiet magnetotail in three dimensions, *J. Geophys. Res.*, *82*, 147, 1977.

Caan, M. N., R. L. McPherron, and C. T. Russell, Solar wind and substorm-related changes in the lobes of the geomagnetic tail, *J. Geophys. Res.*, *78*, 8087, 1973.

Caan, M. N., D. H. Fairfield, and E. W. Hones, Jr., Magnetic fields in flowing magnetotail plasmas and their significance for magnetic reconnection, *J. Geophys. Res.*, *84*, 1971, 1979.

Coroniti, F. V., and C. F. Kennel, Changes in magnetospheric configuration during the substorm growth phase, *J. Geophys. Res.*, *77*, 3361, 1972.

Coroniti, F. V., and C. F. Kennel, Magnetospheric reconnection, substorms, and energetic particle acceleration, in *Particle Acceleration Mechanisms in Astrophysics*, edited by J. Arons, pp. 169–175, American Institute of Physics, New York, 1979.

Coroniti, F. V., L. A. Frank, R. P. Lepping, F. L. Scarf, and K. L. Ackerson, Plasma pulsations in the earth's magnetic tail, *J. Geophys. Res.*, *83*, 2162, 1978.

Cowley, S. W. H., Plasma populations in a simple open model magnetosphere, *Space Sci. Rev.*, *26*, 217, 1980.

Cowley, S. W. H., Magnetospheric asymmetries associated with the Y component of the IMF, *Planet. Space Sci.*, *29*, 79, 1981.

Cowley, S. W. H., The causes of convection in the earth's magnetosphere: A review of developments during the IMS, *Rev. Geophys.*, *20*, 531, 1982.

Cowley, S. W. H., The distant geomagnetic tail in theory and observation, in *Magnetic Reconnection in Space and Laboratory Plasmas*, *Geophys. Monogr. Ser.*, vol. 30, edited by E. W. Hones, Jr., pp. 228–239, AGU, Washington, D. C., 1984.

Cowley, S. W. H., R. J. Hynds, I. G. Richardson, P. W. Daly, T. R. Sanderson, K.-P. Wenzel, J. A. Slavin, and B. T. Tsurutani, Energetic ion regimes in the deep geomagnetic tail: ISEE-3, *Geophys. Res. Lett.*, *11*, 275, 1984.

Crooker, N. U., The magnetospheric boundary layers: A geometrically explicit model, *J. Geophys. Res.*, *82*, 3629, 1977.

Daly, P. W., K.-P. Wenzel, and T. R. Sanderson, Sounding of the plasma sheet in the deep geomagnetic tail using energetic particles, *Geophys. Res. Lett.*, *11*, 1070, 1984*a*.

Daly, P. W., T. R. Sanderson, and K.-P. Wenzel, Survey of energetic ($E > 35$ keV) ion anisotropies in the deep geomagnetic tail, *J. Geophys. Res.*, *89*, 10,733, 1984*b*.

Dungey, J. W., Interplanetary magnetic field and the auroral zones, *Phys. Rev. Lett.*, *6*, 47, 1961.

Dungey, J. W., The length of the magnetospheric tail, *J. Geophys. Res.*, *70*, 1753, 1965.

Fairfield, D. H., On the average configuration of the geomagnetic tail, *J. Geophys. Res.*, *84*, 1950, 1979.

Fairfield, D. H., and N. F. Ness, Configuration of the geomagnetic tail during substorms, *J. Geophs. Res.*, *75*, 7032, 1970.

Farquhar, R. W., and D. W. Dunham, A new trajectory concept for exploring the earth's geomagnetic tail, *J. Guid. Control*, *4*, 192, 1981.

Feldman, W. C., S. J. Schwartz, S. J. Bame, D. N. Baker, J. Birn, J. T.

Gosling, E. W. Hones, Jr., D. J. McComas, J. A. Slavin, E. J. Smith, and R. D. Zwickl, Evidence for slow mode shocks in the distant geomagnetic tail, *Geophys. Res. Lett.*, *11*, 599, 1984.
Frandsen, A. M. A., B. V. Connor, J. V. Amersfoort, and E. J. Smith, The ISEE-C vector helium magnetometer, *IEEE Trans. Geosci. Electr.*, *GE-16*, 195, 1978.
Frank, L. A., and K. L. Ackerson, Several recent findings concerning the dynamics of the earth's magnetotail, *Space Sci. Rev.*, *23*, 375, 1979.
Frank, L. A., K. L. Ackerson, and R. P. Lepping, On hot tenuous plasmas, fireballs, and boundary layers in the earth's magnetotail, *J. Geophys. Res.*, *81*, 5859, 1976.
Garrett, H. B., A. J. Dessler, and T. W. Hill, Influence of solar wind variability on geomagnetic activity, *J. Geophys. Res.*, *79*, 4603, 1974.
Gloeckler, G., F. M. Ipavich, D. Hovestadt, M. Scholer, A. B. Gavin, and B. Klecker, Characteristics of suprathermal H^+ and He^{++} in plasmoids in the distant magnetotail, *Geophys. Res. Lett.*, *11*, 1030, 1984.
Gosling, J. T., D. N. Baker, S. J. Bame, E. W. Hones, Jr., D. J. McComas, R. D. Zwickl, J. A. Slavin, E. J. Smith, and B. T. Tsurutani, Plasma entry into the distant tail lobes: ISEE-3, *Geophys. Res. Lett.*, *11*, 1078, 1984.
Grzedzielski, S., and W. Macek, Comment on the observed plasma densities in Jupiter's distant magnetotail (wake): A possible explanation, *J. Geophys. Res.*, *89*, 2369, 1984.
Hardy, D. A., H. K. Hills, and J. W. Freeman, Occurrence of lobe plasma at lunar distance, *J. Geophys. Res.*, *84*, 72, 1979.
Hayakawa, H., A. Nishida, E. W. Hones, Jr., and S. J. Bame, Statistical characteristics of plasma flow in the magnetotail, *J. Geophys. Res.*, *87*, 277, 1982.
Heikkila, W. J., Magnetospheric topology of fields and currents, in *Magnetospheric Currents*, *Geophys. Monogr. Ser.*, vol. 28, edited by T. A. Potemra, pp. 209–222, AGU, Washington, D. C., 1984.
Holzer, R. E., and J. A. Slavin, A correlative study of magnetic flux transfer in the magnetosphere, *J. Geophys. Res.*, *84*, 2573, 1979.
Hones, E. W., Jr., Transient phenomena in the magnetotail and their relation to substorms, *Space Sci. Rev.*, *23*, 393, 1979.
Hones, E. W., Jr., S. J. Bame, and J. R. Asbridge, Proton flow measurements in the magnetotail plasma sheet made with IMP 6, *J. Geophys. Res.*, *81*, 227, 1976.
Hones, E. W., Jr., D. N. Baker, S. J. Bame, W. C. Feldman, J. T. Gosling, D. J. McComas, R. D. Zwickl, J. A. Slavin, E. J. Smith, and B. T. Tsurutani, Structure of the magnetotail at 220 R_E and its response to geomagnetic activity, *J. Geophys. Res.*, *11*, 5, 1984*a*.
Hones, E. W., Jr., J. Birn, D. N. Baker, S. J. Bame, W. C. Feldman, D. J. McComas, R. D. Zwickl, J. A. Slavin, E. J. Smith, and B. T. Tsurutani, Detailed examination of a plasmoid in the distant magnetotail with ISEE-3, *Geophys. Res. Lett.*, *11*, 1046, 1984*b*.
Howe, H. C. Jr., and J. H. Binsack, Explorer 33 and 35 plasma observations of magnetosheath flow, *J. Geophys. Res.*, *77*, 3334, 1972.
Kamei, T., H. Maeda, and T. Araki, *Auroral Electrojet Indices*, data book 7, pp. 1–7, World Data Center C2, Kyoto University, April 1983.
Klecker, B., M. Scholer, D. Hovestadt, G. Gloeckler, F. M. Ipavich, E. J. Smith, and B. T. Tsurutani, Correlation between proton anisotropy and magnetic field direction in the distant geotail, *Geophys. Res. Lett.*, *11*, 1038, 1984.
Lee, L. C., Z. F. Fu, and S.-I. Akasofu, A simulation study of driven reconnection processes and magnetospheric storms and substorms, *J. Geophys. Res.*, in press, 1985.
Lepping, R. P., M. D. Desch, L. W. Klein, E. C. Sittler, Jr., J. D. Sullivan, W. S. Kurth, and K. W. Behannon, Structure and other properties of Jupiter's distant magnetotail, *J. Geophys. Res.*, *88*, 8801, 1983.
Levy, R. H., H. E. Petschek, and G. L. Siscoe, Aerodynamic aspects of magnetospheric flow, *AIAA J.*, *2*, 2065, 1964.
Lin, R. P., K. A. Anderson, J. E. McCoy, and C. T. Russell, Observations of magnetic merging and the formation of the plasma sheet in the earth's magnetotail, *J. Geophys. Res.*, *82*, 2761, 1977.
Lui, A. T. Y., C.-I. Meng, and S.-I. Akasofu, Search for the magnetic neutral line in the near-earth plasma sheet, 3, An extensive study of magnetic field observations at lunar distances, *J. Geophys. Res.*, *82*, 3603, 1977.
Maezawa, K., Magnetotail boundary motion associated with geomagnetic substorms, *J. Geophys. Res.*, *80*, 3543, 1975.
McPherron, R. L., Growth phase of magnetospheric substorms, *J. Geophys. Res.*, *75*, 5592, 1970.
McPherron, R. L., Magnetospheric substorms, *Rev. Geophys.*, *17*, 657, 1979.
McPherron, R. L., C. T. Russell, and M. P. Aubry, Satellite studies of magnetospheric substorms on August 15, 1968, 9, Phenomenological model for substorms, *J. Geophys. Res.*, *78*, 3131, 1973.
Mihalov, J. D., D. S. Colburn, R. G. Currie, and C. P. Sonett, Configuration and reconnection of the geomagnetic tail, *J. Geophys. Res.*, *73*, 1968.
Mihalov, J. D., D. S. Colburn, and C. P. Sonett, Observations of magnetopause geometry at lunar distance, *Planet. Space Sci.*, *18*, 239, 1970.
Ness, N. F., The earth's magnetic tail, *J. Geophys. Res.*, *70*, 2989, 1965.
Nishida, A., and N. Nagayama, Synoptic survey of the neutral line in the magnetotail during substorm expansion phase, *J. Geophys. Res.*, *78*, 3782, 1973.
Nishida, A., and C. T. Russell, On the expected signatures of reconnection in the magnetotail, *J. Geophys. Res.*, *83*, 3890, 1978.
Nishida, A., H. Haykawa, and E. W. Hones, Jr., Observed signatures of reconnection in the magnetotail, *J. Geophys. Res.*, *86*, 1370, 1981.
Perreault, P., and S.-I. Akasofu, A study of geomagnetic storms, *Geophys. J. R. Astron. Soc.*, *54*, 547, 1978.
Petschek, H. E., Magnetic field annihilation, *NASA Spec. Publ.*, *SP-50*, 325, 1964.
Pilipp, W. G., and G. Morfill, The formation of the plasma sheet resulting from plasma mantle dynamics, *J. Geophys. Res.*, *83*, 5670, 1978.
Propp, K., and D. B. Beard, Cross-tail drift in a realistic model magnetotail, *J. Geophys. Res.*, *89*, 11,013, 1984.
Russell, C. T., Some comments on the topology of the geomagnetic tail, *J. Geophys. Res.*, *82*, 1625, 1977.
Russell, C. T., and R. L. McPherron, The magnetotail and substorms, *Space Sci. Rev.*, *15*, 205, 1973.
Sanderson, T. R., P. W. Daly, K.-P. Wenzel, E. W. Hones, Jr., and S. J. Bame, Energetic ion observations of a large scale vortex in the distant geotail, *Geophys. Res. Lett.*, *11*, 1094, 1984.
Sato, T., R. J. Walker, and M. Ashour-Abdalla, Driven magnetic reconnection in three dimensions: Energy conversion and field-aligned current generation, *J. Geophys. Res.*, *89*, 9761, 1984.
Scarf, F. L., F. V. Coroniti, C. F. Kennel, E. J. Smith, J. A. Slavin, B. T. Tsurutani, S. J. Bame, and W. C. Feldman, Plasma wave spectra near slow mode shocks in the distant magnetotail, *Geophys. Res. Lett.*, *11*, 1050, 1984.
Schindler, K., A theory of the substorm mechanism, *J. Geophys. Res.*, *79*, 2803, 1974.
Scholer, M., D. Hovestadt, B. Klecker, G. Gloeckler, and F. M. Ipavich, Average flow between 70 and 220 R_E in the geomagnetic tail, *Geophys. Res. Lett.*, *11*, 343, 1984*a*.
Scholer, M., G. Gloeckler, D. Hovestadt, B. Klecker, and F. M. Ipavich, Characteristics of plasmoidlike structures in the distant magnetotail, *J. Geophys. Res.*, *89*, 8872, 1984*b*.
Scholer, M., G. Gloeckler, B. Klecker, F. M. Ipavich, D. Hovestadt, and E. J. Smith, Fast moving plasma structures in the distant magnetotail, *J. Geophys. Res.*, *89*, 6717, 1984*c*.
Sibeck, D. G., G. L. Siscoe, J. A. Slavin, E. J. Smith, B. T. Tsurutani, and R. P. Lepping, The distant magnetotail's response to a strong IMF B_y: Twisting, flattening, and field line bending, *J. Geophys. Res.*, *90*, 4011, 1985*a*.
Sibeck, D. G., G. L. Siscoe, J. A. Slavin, E. J. Smith, B. T. Tsurutani, J. T. Gosling, and R. P. Lepping, The distant magnetotail magnetopause and boundary layer, *J. Geophys. Res.*, in press, 1985*b*.
Siscoe, G. L., and W. D. Cummings, On the cause of geomagnetic bays, *Planet. Space Sci.*, *17*, 1795, 1969.
Siscoe, G. L., D. G. Sibeck, J. A. Slavin, E. J. Smith, B. T. Tsurutani, and D. E. Jones, ISEE-3 magnetic field observations in the magnetotail: Implications for reconnection, in *Magnetic Reconnection in Space and Laboratory Plasmas*, *Geophys. Monogr. Ser.*, vol. 30, edited by E. W. Hones, Jr., pp. 240–248, AGU, Washington, D. C., 1984.
Slavin, J. A., and R. E. Holzer, Empirical relationships between interplanetary conditions, magnetospheric flux transfer, and the *AL* index, in *Quantitative Modeling of Magnetospheric Processes*, *Geophys. Monogr. Ser.*, vol. 21, edited by W. P. Olson, pp. 423–436, AGU, Washington, D. C., 1979.
Slavin, J. A., B. T. Tsurutani, E. J. Smith, D. E. Jones, and D. G. Sibeck, Average configuration of the distant (<220 R_e) magnetotail: Initial ISEE-3 magnetic field results, *Geophys. Res. Lett.*, *10*, 973, 1983.
Slavin, J. A., E. J. Smith, B. T. Tsurutani, D. G. Sibeck, H. G. Singer,

D. N. Baker, J. T. Gosling, E. W. Hones, Jr., and F. L. Scarf, Substorm associated traveling compression regions in the distant tail: ISEE-3 geotail observations, *Geophys. Res. Lett.*, *11*, 657, 1984*a*.

Slavin, J. A., E. J. Smith, and D. S. Intriligator, A comparative study of distant magnetotail structure at Venus and earth, *Geophys. Res. Lett.*, *10*, 1074, 1984*b*.

Smith, E. J., A comparison of Explorer VI and Explorer X magnetometer data, *J. Geophys. Res.*, *67*, 2045, 1962.

Smith, E. J., J. A. Slavin, B. T. Tsurutani, W. C. Feldman, and S. J. Bame, Slow mode shocks in the earth's magnetotail: ISEE-3, *Geophys. Res. Lett.*, *11*, 1054, 1984.

Spreiter, J. R., and A. Y. Alksne, Effect of neutral sheet currents on the shape and magnetic field of the magnetosphere, *Planet. Space Sci.*, *17*, 233, 1969.

Stern, D. P., A study of the electric field in an open magnetospheric model, *J. Geophys. Res.*, *78*, 7292, 1973.

Swift, D. W., and L. C. Lee, Rotational discontinuities and the structure of the magnetopause, *J. Geophys. Res.*, *88*, 111, 1983.

Tsurutani, B. T., D. E. Jones, J. A. Slavin, D. G. Sibeck, and E. J. Smith, Plasma sheet magnetic fields in the distant tail, *Geophys. Res. Lett.*, *11*, 1062, 1984*a*.

Tsurutani, B. T., D. E. Jones, and D. G. Sibeck, The two-lobed structure of the distant ($X > 200\ R_e$) magnetotail, *Geophys. Res. Lett.*, *11*, 1066, 1984*b*.

Tsurutani, B. T., D. E. Jones, R. P. Lepping, E. J. Smith, and D. G. Sibeck, The relationship between IMF B_y and the distant tail (150–238 R_e) lobe and plasma sheet B_y fields, *Geophys. Res. Lett.*, *11*, 1082, 1984*c*.

Vasyliunas, V. M., Theoretical models of magnetic field line merging, *Rev. Geophys.*, *13*, 303, 1975.

Villante, U., An overview of Pioneer observations of the distant geomagnetic tail, *Space Sci. Rev.*, *20*, 123, 1977.

Walker, R. C., U. Villante, and A. J. Lazarus, Pioneer 7 observations of plasma flow and field reversal regions in the distant geomagnetic tail, *J. Geophys. Res.*, *80*, 1238, 1975.

Zwickl, R. D., D. N. Baker, S. J. Bame, W. C. Feldman, J. T. Gosling, E. W. Hones, Jr., D. J. McComas, B. T. Tsurutani, and J. A. Slavin, Evolution of the earth's distant magnetotail: ISEE 3 electron plasma results, *J. Geophys. Res.*, *89*, 11,007, 1984.

S.-I. Akasofu, Geophysical Institute, University of Alaska, Fairbanks, AK 99701.

D. N. Baker and R. D. Zwickl, Los Alamos National Laboratory, Los Alamos, NM 87545.

D. G. Sibeck, Department of Atmospheric Sciences, University of California, Los Angeles, CA 90024.

J. A. Slavin and E. J. Smith, Jet Propulsion Laboratory, California Institute of Technology, Pasadena, CA 91109.

(Received February 9, 1985;
revised June 20, 1985;
accepted June 20, 1985.)